Privacy-Preserving Federated Recurrent Neural Networks

Sinem Sav*, Abdulrahman Diaa[†], Apostolos Pyrgelis*, Jean-Philippe Bossuat[‡], and Jean-Pierre Hubaux*[‡]

*École Polytechnique Fédérale de Lausanne (EPFL)

[†]University of Waterloo

[‡]Tune Insight SA

Abstract

We present RHODE, a novel system that enables privacy-preserving training of and prediction on Recurrent Neural Networks (RNNs) in a federated learning setting by relying on multiparty homomorphic encryption (MHE). RHODE preserves the confidentiality of the training data, the model, and the prediction data; and it mitigates the federated learning attacks that target the gradients under a passive-adversary threat model. We propose a novel packing scheme, *multi-dimensional packing*, for a better utilization of Single Instruction, Multiple Data (SIMD) operations under encryption. With multi-dimensional packing, RHODE enables the efficient processing, in parallel, of a batch of samples. To avoid the exploding gradients problem, we also provide several clip-by-value approximations for enabling gradient clipping under encryption. We experimentally show that the model performance with RHODE remains similar to non-secure solutions both for homogeneous and heterogeneous data distribution among the data holders. Our experimental evaluation shows that RHODE scales linearly with the number of data holders and the number of timesteps, sub-linearly and sub-quadratically with the number of features and the number of hidden units of RNNs, respectively. To the best of our knowledge, RHODE is the first system that provides the building blocks for the training of RNNs and its variants, under encryption in a federated learning setting.

I. INTRODUCTION

Collecting and mining sequential data, e.g., time-series, has become the base for numerous real-life applications in the domains of healthcare, energy, and finance. For instance, in personalized healthcare, electrocardiograms (ECGs) are used to monitor patients and to detect heartbeat arrhythmia; and, in finance, historical economic records are mined to forecast stock prices. The state-of-the-art time-series mining is achieved by employing machine learning algorithms that extract useful patterns from the data. A well-known class of algorithms widely used for learning on time-series data is recurrent neural networks (RNNs) [108], [35] and its variants, e.g., Gated Recurrent Units (GRUs) and Long-short Term Memory (LSTMs), that are capable of modelling high-dimensional and non-linear relationships in dynamic systems [111].

Training effective RNNs for time-series tasks requires large amounts of data that are usually generated by multiple sources and scattered across several data holders. Sharing or centralizing this data is difficult because it is privacy sensitive [133]. For example, smart-meter data might leak householders' identities [20] and their activities [92], location data reveal information about peoples' lifestyles and beliefs [118], [117], [97], [132], and healthcare time-series are by nature very private information [13], [77]. Additionally, privacy regulations enforce strict rules for sharing this type of data [1], [5]. As a result, privacy-preserving data sharing and collaborative machine learning solutions have gained a significant importance [77], [18], [55].

Federated learning (FL) is a machine learning paradigm that enables privacy-preserving collaborative training of machine learning models. With FL, data holders retain their data in their own premises and share model updates with an aggregation server that coordinates the learning over their joint data [81], [69], [68]. FL has been applied in many time-series applications by using RNNs to forecast the energy load [36], to detect out-of-vocabulary words [24], to predict the next word typed on mobile phones [49], and to classify cancer in healthcare systems [42]. Although FL provides collaborative learning without data sharing, it still raises privacy issues: The shared intermediate model is vulnerable to privacy attacks that can reconstruct parties' input data or infer the membership of data samples in the training set, hence needs to be protected during the training process [53], [126], [139], [85], [95], [136], [44], [61], [125], [32], [34]. Moreover, it was recently shown that RNNs are particularly vulnerable to inference attacks (e.g., membership inference) compared to traditional neural networks [130].

To overcome these shortcomings, several works propose integrating protection mechanisms such as differential privacy (DP), secure multiparty computation (SMC), or homomorphic encryption (HE) in the FL process. Each of these techniques, however, introduces a different trade-off: DP solutions decrease the utility of the machine learning model — in particular for RNNS [130] — while their level of practical privacy protection remains unclear [59]; SMC solutions lack scalability in terms of circuit complexity and number of parties due to high communication overheads [47], [65]; and HE solutions do not scale with the model complexity due to high computational overhead. Recently, a multifaceted approach, termed multiparty homomorphic encryption (MHE) [39], [11], where the private key is secret-shared among the data holders, has been used by several works to better balance the aforementioned trade-offs with privacy-preserving federated learning [40], [110]. However, these solutions focus solely on the training of generalized linear models or feed-forward neural networks and do not tackle the training of RNNs, which introduces its own additional challenges: (i) the sequential computations make the training procedure slow and hard to parallelize, and (ii) the long-term dependencies lead to exploding (or vanishing) gradients [100], [14].

By improving upon MHE-based works [40], [110], we build Rhode, a novel system that enables the training of and predictions on RNNs and its variants in a cross-silo federated learning setting with N data holders by performing all the computations under homomorphic encryption. Rhode protects the confidentiality of the training data, the local gradients, and the global model and under a passive adversary model (a common assumption for cross-silo settings) that allows collusions of up to N-1 data holders. To achieve this, both the local

gradients and the FL model remain encrypted throughout the RHODE's collective training pipeline. Hence, RHODE mitigates passive FL attacks that target the gradients or the global model by concealing all operations throughout the learning. To accelerate RNN training, RHODE enables mini-batch training by relying on a novel packing scheme that reduces the processing time of a batch. To address the problem of exploding/vanishing gradients, RHODE uses efficient polynomial approximations of the gradient clipping function. After training, RHODE enables predictions-as-a-service (PaaS) to a querier that obliviously evaluates the trained model on its private inputs and obtains the prediction results. We implement RHODE and our experimental evaluation shows that its accuracy is on par with non-secure centralized and decentralized solutions. Moreover, it scales sub-linearly with the number of features, sub-quadratically with the hidden RNN dimension, and linearly with the timesteps, the batch size and the number of data holders. For example, RHODE can process 256K samples distributed among 10 data holders with an RNN of 32 hidden units and 4 timesteps, with 100 global iterations during training, in ~ 1.5 hours.

In summary, our contributions are the following:

- We present RHODE, a novel system for the training of RNNs in a FL setting by relying on multiparty homomorphic (MHE) encryption. By using MHE, RHODE conceals all intermediate values and the model that are communicated in the FL process. After training, RHODE enables oblivious predictions to a querier that provides its encrypted inputs.
- We design a novel multi-dimensional packing scheme that enables efficient encrypted matrix operations suitable for mini-batch training. We show that performing matrix multiplication with our scheme improves the state-of-the-art [60] in terms of throughput proportionally to the dimension of the matrices. Moreover, our packing scheme preserves the number and size of the cryptographic keys regardless of the matrix size.
- We propose and evaluate various polynomial approximations for performing gradient clipping under encryption to alleviate the problem of vanishing/exploding gradient that is inherent to RNNs.
- We experimentally evaluate RHODE and show that:
- It scales sub-linearly with the number of features, sub-quadratically with the hidden RNN dimension, linearly with the timesteps
 or the batch size, and sub-linearly (or linearly) with the number of data holders depending on the number of samples in the dataset.
- Its homomorphic operations and building blocks have negligible effect on the model performance for common time-series forecasting benchmarks, with both homogeneous and heterogeneous (imbalanced) data distribution among the data holders.

To the best of our knowledge, RHODE is the first system that enables the training of and prediction on sequential data with RNNs in a federated learning setting under encryption. Our system mitigates passive FL inference attacks during training and preserves the privacy of the data holders' data, the intermediate model/gradients communicated through network, the querier's evaluation data, and the final model.

II. RELATED WORK

We review the related work on privacy-preserving time-series, as well as on privacy-preserving federated training of, and prediction on machine learning models.

A. Privacy-Preserving Time-Series

Previous works aiming to protect the privacy of time-series data employed secure aggregation techniques to enable the computation of simple statistics and analytics [70], [84], [104], whereas others combined secure aggregation with differential privacy to bound the leakage stemming from the computations [113], [19]. More recently, Liu et al. [76] employed secure multi-party computation (SMC) techniques for privacy-preserving collaborative medical time-series analysis, based on dynamic time warping. Dauterman et al. [31] use function secret sharing (FSS) to support various functionalities, e.g., multi-predicate filtering, on private time-series databases. All these authors focus on simple collaborative time-series tasks and not on the privacy-preserving training of machine learning models on time-series data, which is the main focus of this work.

B. Privacy-Preserving Federated Training of Machine Learning Models

Federated learning (FL) enables different data holders to perform the collective training of a machine learning model while maintaining the data in their local premises and communicating only the intermediate values/local model updates to an aggregation server [81], [69], [68]. Similarly to tabular or image data, FL was applied on many time-series applications such as load forecasting [36], natural language processing [24], [49], traffic flow prediction, [78], and healthcare systems [42]. However, recent research has shown that sharing gradients and local model updates in FL lead to severe privacy leakage because membership inference and data/label reconstruction attacks are effective [53], [126], [139], [85], [95], [136], [44], [61], [125], [32], [34].

One common approach for privacy-preserving *decentralized* or *federated* machine learning is to integrate differential privacy (DP) into the learning phase such that the intermediate values exchanged among the data holders and the global model meet the DP requirements [115], [72], [7], [82], [127], [129]. McMahan et al. recently applied DP to recurrent neural network models to protect user-level privacy [83], and Wen et al. applied local differential privacy to a FL framework for energy-theft detection [128]. However, DP introduces a privacy vs. utility trade-off that is hard to parameterize thus hindering its deployment. For RNNs in particular, Yang et al. also show that perturbing either the gradients during training or the model weights after training to achieve DP guarantees results in higher utility loss than alternative neural

networks [130]. Another line of research applies secure multiparty computation (SMC) for improving the privacy guarantees of decentralized machine learning [96], [43], [45], [9], [112], [16], [27], [91], [8], [90], [123], [124], [25], [21], [23], [67], [120]. Other works combine SMC with DP to improve enable privacy-preserving FL [59], [122]. Overall, these solutions enable the training of regression models and feed-forward neural networks, whereas RNNs or its variants have not been studied. As a result, several algorithms, e.g., back-propagation through time, and crucial operations, e.g., gradient clipping, have not been addressed. One recent work, which relies on additive secret-sharing, investigated the training of recurrent neural networks as a case study [135], but without evaluating runtime performance or scalability.

Several works employ homomorphic encryption (HE) to either enable secure aggregation in decentralized learning [102], [103] or to encrypt the clients' data, before outsourcing it to a server that performs the model training [134]. Zheng et al. use MPC in combination with HE for maliciously secure federated training [138], [137]. None of these works, however, address the learning of sequential patterns over the data. A recent study employs secure aggregation with HE for federated traffic flow prediction [78], but the study remains vulnerable to privacy attacks due to the shared global model. To balance the trade-off between privacy, utility, and performance, several works apply multiparty homomorphic encryption (MHE) [11] to realize decentralized trust and to enable efficient collaborative homomorphic operations, such as collective bootstrapping [94]. In particular, recent works apply MHE to federated learning to conceal any information exchanged during the learning process, including the model and any intermediate values [40], [110] and demonstrate their real-life applications [41], [109]. However, their focus is on generalized linear models [40] or feed-forward neural networks [110], and not the training of RNNs. For instance, the packing scheme and the matrix/vector operations employed in [110] are tailored for the processing of a single sample (to eliminate explicit transpose and matrix multiplications and to enable vector-matrix multiplications). Whereas in this work, we propose a novel packing scheme suitable for mini-batch training of RNNs and enable the matrix transpose and matrix multiplications. Moreover, we propose several polynomial approximations for enabling critical operations for RNNs, such as gradient clipping, under MHE.

A different line of research is focused on the private aggregation of teacher ensembles (PATE) [98], [99], and its variants [79], [131]; the focus is mainly on knowledge transfer by combining differential privacy and generative adversarial networks (GANs). PATE enables the private training of a student model from several teacher models, where the knowledge is transferred in a noisy fashion. However, PATE requires a trusted aggregator, and although it achieves record-level differential privacy guarantees, it remains vulnerable to property inference attacks [85]. Our line of research diverges from these works due to their strong assumption of publicly available datasets and their different designs that target knowledge transfer. Choquette-Choo et al. recently proposed CaPC Learning that enables confidential and private collaborative learning by relying on MPC, HE, and DP, in order to increase the utility of each data holder's local machine learning model [29]. Their approach works on non-iid settings with heterogeneous model architectures across parties. However, CaPC Learning is evaluated only on feed-forward neural networks and the number of parties needs to be large enough to obtain better utility and higher privacy guarantees. Our work decouples privacy from the amount of data or the number of parties by relying on MHE.

RHODE enables the training of RNNs in the federated learning while protecting the confidentiality of the training data of each data holder, the local gradients, and the global model. By design, RHODE mitigates passive FL inference attacks during training, as all intermediate values that are exchanged between data holders remain encrypted and as it enables all the computations of the FL pipeline under encryption.

C. Privacy-Preserving Prediction on Machine Learning Models

Privacy-preserving prediction on machine learning models plays an important role for Prediction-as-a-Service (Paas) solutions whose aim is to protect the model from the client (who queries the model) and the client's evaluation data from the service provider. A series of works employ MPC or HE (or a combination of them) to enable privacy of both the data and the model holder [46], [75], [62], [101], [107], [88], [6], [15], [52], [106]. These works, however, develop and improve cryptographic primitives that support the evaluation of feed-forward neural networks. Only a few recent studies focus on privacy-preserving prediction on RNNs and its variants. Bakshi and Last propose CryptoRNN; it employs HE but requires interaction between the client and the server in order to refresh the ciphertexts [12]. Rathee et al. propose SiRNN that relies on novel two-party computation (2PC) protocols and lookup tables, combined with an iterative algorithm, to approximate non-linear math functions [105]. Feng et al. tackle privacy-preserving natural language processing [38] by relying on MPC. And Feng et al. propose a hybrid approach that combines HE and garbled circuits for evaluating GRU networks on text analysis tasks [37]. More recently, Jang et al. have extended the CKKS-HE scheme to the multi-variate ring learning with errors (RLWE) problem in order to support efficient matrix operations that are required for evaluating GRUs on sequence modeling, regression, and classification tasks [58]. Similar to these works, RHODE protects the confidentiality of the model and the client's evaluation data during the prediction phase. However, our work is broader, as it enables both the federated training of and prediction on RNNs by relying on MHE.

III. BACKGROUND

A. Multiparty Homomorphic Encryption (MHE)

In this work, we rely on a multiparty fully-homomorphic encryption (MHE) scheme in order to enable distributed cryptographic operations across the data holders. We employ the multiparty variant of Cheon-Kim-Kim-Song (CKKS), a leveled homomorphic-encryption scheme based on the *ring learning with errors* (RLWE) problem [26], that is proposed by Mouchet et al. in [94]. This scheme is secure against

Algorithm 1 Federated Averaging Algorithm (FedAvg)

```
1: Initialize the global model W^0
                                                                                                                                                    ⊳ Server executes
2: for k = 0 \rightarrow e - 1 do
                                                                                                                                                   Choose S random subset of N data holders
3:
       Send W^k to each data holder in S
4:
      Each data holder S_i in S executes (in parallel):
5:
        for \ell = 0 \rightarrow l - 1 do
                                                                                                                                                     W_{\scriptscriptstyle i}^{k+1}\!\leftarrow\! \mathsf{Local}\;\mathsf{Gradient}\;\mathsf{Descent}(\cdot)
6:
7:
8:
```

post-quantum attacks, enables floating-point arithmetic, and tolerates collusions of up to N-1 parties, under a passive threat model. Below, we summarize the most important operations of this scheme:

- **Key Generation:** Each data holder i locally generates a secret key (sk_i) . The public key (pk) and evaluation keys ([ek]) are collectively generated from the data holders' local secret keys $(\mathsf{CKeyGen}([sk_i]))$. [ek] is a set of special public keys that are required for the execution of homomorphic multiplications and rotations. With this scheme, any data holder can encrypt and locally perform homomorphic operations by using pk and [ek], but decrypting a ciphertext requires the collaboration among all data holders $(\mathsf{CDecrypt}(\mathbf{c}_{pk},[sk_i]))$. We denote any ciphertext encrypted under pk with bold-face \mathbf{c}_{pk} throughout this paper. When there is no ambiguity, we omit the sub-index and use \mathbf{c} .
- Arithmetic Operations and Parallelization: The CKKS homomorphic encryption scheme enables approximate arithmetic over a vector of complex numbers ($\mathbb{C}^{\mathcal{N}/2}$) for a polynomial ring of dimension \mathcal{N} . Encrypted operations over $\mathbb{C}^{\mathcal{N}/2}$ are carried out in a Single Instruction Multiple Data (SIMD) manner, which enables parallelization over the $\mathcal{N}/2$ plaintext vector slots.
- Arithmetic Circuit Depth and Collective Bootstrapping: A fresh ciphertext has an initial level of \mathcal{L} and at most \mathcal{L} multiplications (i.e., an \mathcal{L} -depth circuit) can be evaluated on this ciphertext. When the levels are exhausted, the ciphertext is refreshed with a collective bootstrapping operation (CBootstrap($\mathbf{c}_{pk},[sk_i]$)) that enables further operations. We note here that CBootstrap(\cdot) is a costly operation with approximately 2 orders of magnitude higher overhead than a homomorphic addition/multiplication.
- Slot Rotations: The slots of a ciphertext vector can be re-arranged via rotations to the left or right, i.e., $RotL/R(\mathbf{c}_{pk},k)$ homomorphically rotates \mathbf{c}_{nk} to the left/right by k positions using [ek].
- Collective Key-Switch: This operation (CKeySwitch($\mathbf{c}_{pk},pk',[sk_i]$)) changes the encryption key of a ciphertext \mathbf{c} from pk to pk'. As such, only the holder of the secret key corresponding to pk' can decrypt the result $\mathbf{c}_{pk'}$.

Note that the aforementioned operations are MHE ones if they are termed as 'collective' (or if the operation name starts with C, e.g., $CKeyGen(\cdot)$), otherwise they are pure CKKS functionalities. For further details about the CKKS scheme, e.g., relinearization and rescaling, we refer the reader to the original work of Cheon et al. [26], and for more information about the collective MHE operations to the work of Mouchet et al. [94].

B. Federated Learning

Federated Learning (FL) is an emerging collaborative machine learning approach that enables multiple data holders to train a model without sharing their local data [81], [69], [68]. With FL, each data holder performs several training iterations on its local data, and the resulting local models are aggregated into a global model via an aggregation server. We summarize the most popular federated learning algorithm, i.e., FedAvg, proposed by McMahan et al. [81] in Algorithm 1. W_i^k denotes the model weights of the i^{th} data holder during the k^{th} iteration. If no sub-index is used, then it simply denotes the global model weights at a certain iteration. The server initializes the model weights, sends them to a random subset of data holders S that execute the local gradient descent algorithm (Local Gradient Descent(·); see Section IV-B for the details of the algorithm when it is tailored for RNN execution under encryption with RHODE) to update their local model. The model updates from each data holder are aggregated to the global model via weighted averaging (n_i denotes the number of local samples at the i^{th} data holder and n the total number of samples). The number of global and local iterations are denoted as e and e, respectively. Note that FedAvg is a generalization of the standard FedSGD algorithm with several number of local iterations on each data holder's side.

C. Recurrent Neural Networks

Recurrent neural networks (RNNs) are a special type of models that enable learning on sequential data (e.g., time-series) [108], [35]. A typical RNN is composed of an input layer that obtains the sequential input to the network, a hidden layer, and an output layer. Contrary to feed-forward neural networks where the information flows from the input to the output layer, in an RNN, the information is fed back to the network through connections between its nodes that form a directed graph. The RNN input is a sequence where each item in the sequence is called a timestep. The hidden layer consists of several hidden units (neurons). Each hidden unit has a hidden state that retains the information from the previous timestep. Thus, RNNs capture sequential patterns in the data by processing each timestep sequentially and updating the hidden state. In this way, RNNs use earlier information in the sequence to learn the current output and retain a form of *memory*.

A typical RNN, e.g., an Elman Network [35], takes a sequential input $(X = x_1, x_2, \dots, x_T)$ of T timesteps and outputs the prediction y_t through the hidden units and an activation function by sequentially computing the hidden state at time t as

$$h_t = \varphi(h_{t-1} \times W + x_t \times U + b_h)$$

$$y_t = h_t \times V + b_y$$
(1)

where U,W, and V denote the input-to-hidden, hidden-to-hidden, and hidden-to-output weight matrices, respectively, and b_h and b_y the hidden and output biases. φ is the activation function that is usually chosen to be Tanh. Note that the input or the input batch at each timestep x_t can be itself a d-dimensional feature vector (or a matrix $b \times d$ for a batch of size b). But to avoid notation overflow, we assume that each timestep is a scalar value throughout the paper, unless otherwise stated. The dimensions of U,W, and V are $d \times h, h \times h$ and $h \times o$, where d,h, and o are the input, hidden, and the output dimensions, respectively.

Similarly to feed-forward neural networks, the training of RNNs is an iterative process with a series of forward and backward passes. The forward pass comprises the prediction by using the formulas in Eq. 1. However, back propagation is computed via the back-propagation through time (BPTT) algorithm that takes into account the error propagated through the hidden units and computes the gradients by following the chain rule [108]. We describe in detail the operations of this process under RHODE in Section IV-B, Algorithm 2.

Finally, we note that there are various RNN structures, i.e., one-to-one, one-to-many, many-to-one, and many-to-many, depending on the input and output layer size (e.g., a many-to-many structure yields outputs for κ timesteps). Configuring RHODE to support these is trivial and requires simple alterations in its implementation. However, RNN variants in terms of architecture, such as Gated Recurrent Unit (GRU) or Long Short-Term Memory (LSTM), require several changes to the hidden units, e.g., to account for memory units in LSTM. Throughout this paper, we consider the traditional RNN architecture that is called simple, vanilla, or an Elman RNN [35]. A detailed discussion about how to extend RHODE for other RNN architectures is given in Appendix B.

IV. RHODE DESIGN

We introduce the problem and the overview of our solution. We also present the challenges associated with RNN training.

A. Problem Statement

We first discuss the system and threat model of RHODE, as well as its training and prediction objectives.

System Model. We consider a cross-silo federated learning (FL) setting with a moderate number of data holders (N) (typically in the range of 2 to 200 [63]). The data holders are interconnected and organized in a tree-structured topology for efficient communication (although our system can be easily adapted to any network topology). Each data holder i has its time-series input data X^i and the corresponding output Y^i ($Y^i \in \{0,1,\cdots,n\}$ for n-class classification or $Y^i \in \mathbb{R}$ for regression tasks) that they contribute for training a joint machine-learning model (horizontal FL). After training, the data holders use the model to enable predictions-as-a-service (PaaS) for a querier q with evaluation data X^q . The querier can be one of the N data holders or an external entity and obtains Y^q , the prediction result.

Threat Model. We assume a passive-adversary threat model that allows collusions between up to N-1 parties, including the data holders and the querier. As such, the data holders follow the protocol, but up to N-1 of them can collude and share their observations or their inputs to extract information about the other data holder's inputs. RHODE aims at preserving the confidentiality of both the input data and the model during the training and prediction pipelines. We note here that our focus is on mitigating FL inference attacks that target the model during training. Inference attacks targeting the system's outputs during prediction, e.g., model stealing, are out of the scope of this work. We discuss complementary security mechanisms that can be used orthogonally to RHODE to mitigate such attacks in Appendix B. Note that although RHODE's system and threat model is widely used in the literature [40], [110], [43], [45], [9], [112], [27], [91], [8], [25], [120], the functionality and the underlying protection mechanism differ from them; our main focus is on RNNs by relying on MHE.

Training. The data holders aim at collaboratively training an RNN model *without* relying on a trusted party and *without* revealing their data to any other data holder. RHODE's objective is to enable this and to mitigate passive FL attacks that target the model or local gradients by protecting the confidentiality of the data holders' inputs, the model, and any intermediate values, e.g., local or global models, that are communicated in the system. As we optimize the communication via a tree-structured topology, the root data-holder plays the role of the aggregation server in traditional FL, and for clarity, throughout the paper, we refer to this node as the *aggregation server*.

Prediction. RHODE's objective is to protect the confidentiality of both the querier's data and the trained RNN model, i.e., the data holders should not learn anything about the querier's evaluation data and the querier should not learn anything about the model other than what it can learn from the prediction output.

B. Solution Overview

To fulfill the training and prediction objectives under the given threat model, RHODE relies on FL and MHE. For clarity, we refer to Algorithm 1 to explain our high-level protocol. Note that RHODE enables, under encryption, both FedAvg and FedSGD with every data holder included in each iteration (i.e., |S| = N) since we consider a cross-silo setting and given that all data holders are available to participate

Algorithm 2 Local Computation Phase (RNN)

```
Input: U, W, V, h_{prev}, X = (x_1, x_2, \dots, x_t), Y = (y_1, y_2, \dots, y_t)
         Output: \nabla U, \nabla W, \nabla V
  1: loss \leftarrow 0
 2: \mathbf{h}_0 \leftarrow \mathbf{h}_{prev}
  3: \ \mathbf{for} \ t \!\leftarrow\! 1 \!:\! T \ \mathbf{do}
                                                                                                                                                                                                                                                                                                                                          ⊳ Forward Pass
                  \mathbf{z}_t \leftarrow \mathbf{h}_{t-1} \times \mathbf{W} + x_t \times \mathbf{U}
 5:
                  \mathbf{h}_t \leftarrow \varphi(\mathbf{z}_t)
                  \mathbf{p}_t \leftarrow \mathbf{h}_t \times \mathbf{V}
  7: end for
 8: \mathbf{h}_{prev} \leftarrow \mathbf{h}_t
 9: \mathbf{dh}_{next} = \mathbf{0}
10: \nabla \mathbf{U}, \nabla \mathbf{W}, \nabla \mathbf{V} = \mathbf{0}
11: for t \leftarrow T : 1 do
                                                                                                                                                                                                                                                                                                                                      \mathbf{dy} \!\leftarrow\! \mathbf{p}_t \!-\! y_t
12:
                  \mathbf{dh} \leftarrow \mathbf{dy} \times \mathbf{V}^T + \mathbf{dh}_{next}
13:
14:
                  \mathbf{dz} \leftarrow \mathbf{dh} \odot \varphi'(\mathbf{z}_t)
                  \mathbf{dh}_{next}\!\leftarrow\!\mathbf{dz}\!\times\!\mathbf{\hat{W}}^{T}
15:
                   \nabla \mathbf{V} \leftarrow \nabla \mathbf{V} + \mathbf{h}_t \otimes \mathbf{dy}
16:
                   \nabla \mathbf{U} \leftarrow \nabla \mathbf{U} + x_t \otimes \mathbf{dz}
17:
18:
                   \nabla \mathbf{W} \leftarrow \nabla \mathbf{W} + \mathbf{h}_{t-1} \otimes \mathbf{dz}
19: end for
```

in cryptographic operations (see Appendix B for a possible extension to the asynchronous learning case). By enabling RNN training, RHODE handles learning over sequential data in general yet, throughout the paper, our main focus is on time-series data.

To mitigate the passive FL inference attacks during training, RHODE retains the model and all the intermediate values communicated through the network in encrypted form. However, keeping the model protected implies that all the local RNN operations performed by the data holders need to be carried out under homomorphic encryption. To efficiently enable this, RHODE uses a novel packing strategy and several cryptographic optimizations that are detailed in Section V.

1) Private Training: The training protocol of RHODE operates in four phases: Setup, Local Computation, Aggregation, and Model-Update. We detail these phases hereunder:

Setup Phase: In this phase, the necessary cryptographic and learning parameters are decided by the data holders, i.e., the minimum security guarantees, the RNN architecture, and the learning parameters, e.g., the learning rate (η) , the batch size (b), and the number of global (e) and local iterations (l). Then, the data holders generate their secret keys (sk_i) , for the i^{th} data holder) and collectively generate the corresponding public key (pk) with the forenamed MHE scheme (Section III-A). For the training execution to start, the aggregation server initializes the global model (Line 1, Algorithm 1), encrypts it with pk, and broadcasts it to all data holders.

Local Computation Phase: Each data holder receives the encrypted global model weights and begins the local gradient descent (Local Gradient Descent(·), Line 6, Algorithm 1), i.e., the execution of the forward and backward pass on its local data as detailed in Algorithm 2 for a simple many-to-many RNN with $\kappa = T$ outputs. Note that for different RNN architectures, the local gradient descent algorithm can be altered (see Appendix B for an example of the Local Computation Phase for a Gated Recurrent Unit (GRU) architecture). We denote the encryption of any value, vector, or matrix with bold-face, e.g., \mathbf{W} , and for clarity, we omit the indices of the global iteration and the data holder in Algorithm 1. x_t is the input feature-vector for a specific timestep (or a matrix of size $b \times d$ for a batch of size b, in which case the outer-vector products in the backward pass become matrix multiplications) and y_t the corresponding output(s). φ (φ') indicates any type of activation function (and its derivative), e.g., Tanh or Sigmoid. We denote the transpose of a matrix A as A^T , the element-wise multiplication with \odot , the matrix or vector multiplication with \times , and the outer product with \otimes . Note that the characteristics of RNNs incur several challenges when training them under encryption and choosing appropriate solutions is crucial. We discuss these challenges in Section IV-C and propose several techniques and optimizations to alleviate them in Section V.

Aggregate Phase: Data holders collectively aggregate their locally computed models (or gradients) in a tree-manner. That is, each data holder sends its (encrypted) local model to its parent, and each parent homomorphically sums the received child-models with its own. As such, the aggregation server receives the sum of the local models and updates the global model.

Model-Update Phase: The aggregation server updates the global model by averaging the local models of the data holders (Line 8, Algorithm 1). At this phase, the aggregation server also applies gradient clipping (see Section V-B for details). We assume that the batch size is public information (and agreed upon in the Setup Phase), hence the division for averaging over the encrypted local models becomes a multiplication with a plaintext value. The global model is then broadcast to all data holders for the next Local Computation Phase.

Overall, the model training composes the Local Computation, Aggregate, and the Model-Update Phases, which are repeated for a predefined *e* number of global iterations.

2) Predictions-as-a-Service (PaaS): After the collective model training, the data holders can (i) use the encrypted model for oblivious PaaS without decryption, or (ii) if required by the application, they can collectively decrypt the model and reveal it to all the data holders and/or an external party for semi-oblivious PaaS. In both cases, the querier's evaluation data is encrypted with the data holders' collective public key and we rely on the collective key-switch functionality of the underlying MHE scheme (Section III-A). In particular, for (i), the querier encrypts X^q with the data holders' collective key pk, the data holders then compute the prediction on the encrypted data using the encrypted model, and switch the encryption key of the result with $CKeySwitch(X^q_{pk},qk,[sk_i])$), where qk is the querier's key. As such, only the querier can decrypt the prediction result. For (ii), the collective decryption is simply a special case of the collective key-switch operation with the encrypted model as input and no target public key. The rest of the evaluation is same as oblivious PaaS.

C. Challenges Associated with RNN Training

We discuss the challenges, as well as several solutions, associated with the training of RNNs in general. We also highlight how these challenges (and their solutions) further increase the difficulty of RNN training under homomorphic encryption. Section V presents the building blocks that RHODE presents to alleviate these challenges.

RNNs are inherently difficult to train because of their sequential operations, i.e., the computations performed over the timesteps or, in other words, the dependency of each network node on the output of its previous one. This phenomenon causes two issues when training RNNs: (i) the training procedure is slow, complex, and hard to parallelize, and (ii) the gradients tend to explode (or vanish) due to long-term dependencies between timesteps; during the execution of the back-propagation through time (BBPT) algorithm they are computed based on numerous consecutive matrix multiplications according to the chain rule [100], [14].

To mitigate the first challenge, several works suggest accelerating RNN training through data parallelization, i.e., via a distributed approach and/or mini-batch training [66], [114], [57]. For example, a master-slave approach where slave machines first compute the gradients and then a master machine aggregates them to perform the global update (Map-Reduce algorithm [30]) is commonly proposed. RHODE ensures similar efficiency to such distributed training-based approaches, through federated learning that is, by definition, distributed and resembles the master-slave relationship proposed for distributed RNNs. On the other hand, mini-batch training under homomorphic encryption requires a well-suited packing scheme for efficient matrix multiplication and transpose operations. Therefore, in Section V-A, we propose a novel multi-dimensional packing scheme that reduces the processing time over a large batch.

The second challenge of exploding or vanishing gradients is addressed in the literature by several techniques such as the use of gating mechanisms, e.g., LSTMs [54], along with a possible modification of the gradient propagation [64], encoder-decoder approaches [28], gradient clipping [100], non-saturating functions [22], and various recurrent-weight initialization techniques via identity or orthogonal matrix initialization [71], [51]. Extending RNNs to LSTMs as a solution to the problem of exploding/vanishing gradients brings its own challenges, due to the computational complexity of training LSTMs under homomorphic encryption, and we describe a similar extension in Appendix B. Although various weight-initialization techniques are straightforward to adopt, the most widely applied solution, i.e., gradient clipping, is not easy to compute under encryption as it requires a comparison function that is not homomorphically enabled. Therefore, in Section V-B, we present various approximations for the efficient computation of an element-wise clipping function, through different polynomials.

V. CRYPTOGRAPHIC BUILDING BLOCKS

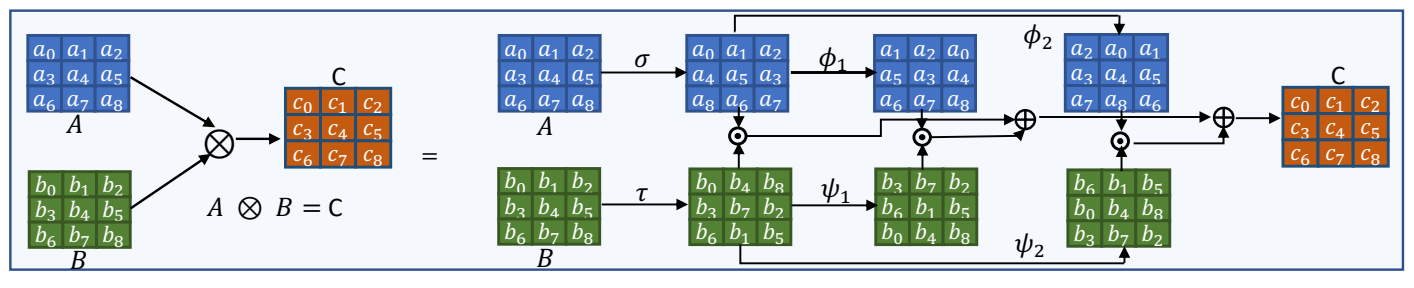
We detail the main cryptographic building blocks that enable the training of and prediction on RNNs in RHODE. We describe the packing scheme and the optimized matrix operations including the matrix-multiplication and matrix-transpose in Section V-A and the approximated neural network building blocks in Section V-B. Then, we present guidelines for configuring several cryptographic parameters in Section V-C and we analyze RHODE's security in Section V-D.

A. Packing and Optimized Matrix Operations

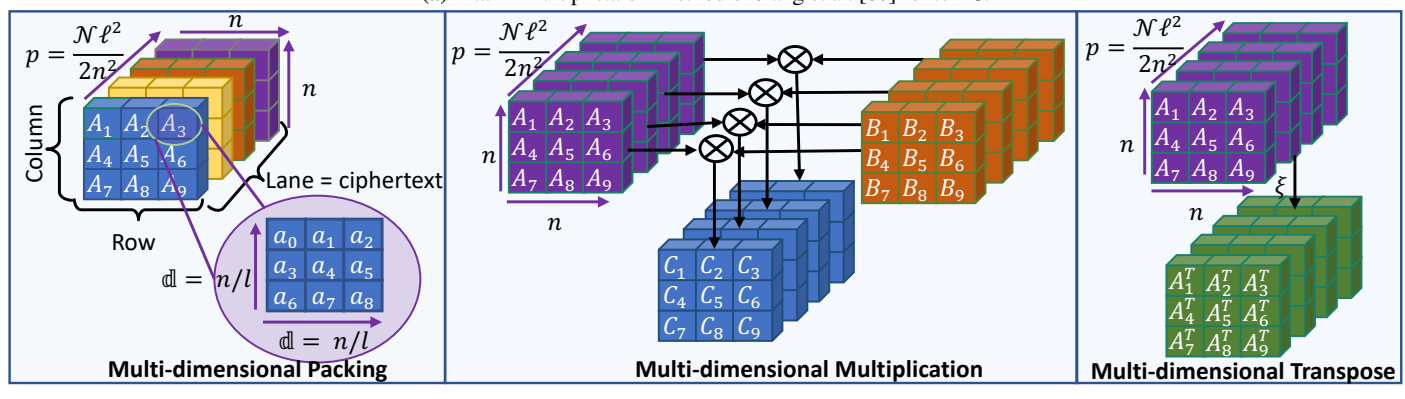
We present the packing scheme and the optimized matrix operations used for RNN training in RHODE. Due to the use of FHE, packing has a significant effect on the training performance as through SIMD operations, it enables mini-batch training which alleviates the inherent high training times of RNNs. In addition, matrix operations are the most heavy and frequent operations in RNNs (see Lines 4-6 and 13-18 in Algorithm 2). Thus, optimizations of the packing scheme and matrix operations such as multiplication or transpose, are crucial for RHODE's efficient training execution. In this work, we rely on a row-based packing approach where matrices are decomposed row-wise and packed in one plaintext and we use Jiang et al.'s [60] approach as a baseline for the matrix operations. On top of these matrix operations and row-based packing, we propose and implement a novel multi-dimensional packing scheme that relies on block matrices¹ and the matrix operations that are described below, for further optimizations.

Matrix Multiplication. The typical methods for matrix multiplication in fully homomorphic encryption (FHE) [48], [89] do not preserve the structure of the matrix in the plaintext slots, i.e., the shape of the computation output is different than that of the inputs, or one of the

¹Block matrix is a matrix defined by sub-matrices, called blocks, which enable matrix operations in parallel.



(a) Matrix Multiplication Method of Jiang et al. [60] for n = 3.



(b) An overview of our Multi-dimensional Packing scheme, its Multiplication and Transpose operations.

Figure 1: Schematic Overview of the (a) Matrix Multiplication Protocol by Jiang et al. [60] and (b) our Multi-dimensional Packing Scheme.

matrices is encoded in diagonal form. This prevents efficient chaining of matrix operations since after each multiplication an expensive linear transformation is required to convert the output back to an encoding compatible with further operations.

Jiang et al. propose a method for matrix multiplication that preserves the format of row-encoded matrices, enabling the efficient chaining of an arbitrary number of matrix operations [60]. With their approach, a matrix multiplication consumes 3 *levels* per multiplication (2 if one matrix is in plaintext) due to 2 linear transformations and 1 dot product. However, it enables the packing of multiple matrices in a single ciphertext (assuming the number of entries of the matrix is smaller than $\mathcal{N}/2$) and to operate on them in a SIMD manner, which increases efficiency and compensates for the *level* consumption. This feature yields a favorable balance between computation runtime and level consumption for RNN computations. We now describe this format-preserving method for matrix multiplication that is illustrated in Figure 1a. Given A and B, matrices of size $n \times n$, the multiplication $C = A \otimes B$ can be evaluated under encryption as the scalar product $\mathbf{C} = \langle \tilde{\mathbf{A}}, \tilde{\mathbf{B}} \rangle$, where $\tilde{\mathbf{A}}$ and $\tilde{\mathbf{B}}$ are size-n vectors of permutations of \mathbf{A} and \mathbf{B} , respectively (or permutations of the original matrices \mathbf{A} and \mathbf{B}). These permutations are represented by the linear transformations σ (cyclic rotation of all columns, where the i-th column is rotated by i positions), ϕ_i (cyclic rotation of all columns by i positions). For example, if A and B are two 4×4 matrices, then $\tilde{\mathbf{A}} = \{\phi_0(\sigma(\mathbf{A})), \phi_1(\sigma(\mathbf{A})), \phi_2(\sigma(\mathbf{A})), \phi_3(\sigma(\mathbf{A}))\}$ and $\tilde{\mathbf{B}} = \{\psi_0(\tau(\mathbf{B})), \psi_1(\tau(\mathbf{B})), \psi_2(\tau(\mathbf{B})), \psi_3(\tau(\mathbf{B}))\}$, and $\mathbf{C} = \langle \tilde{\mathbf{A}}, \tilde{\mathbf{B}} \rangle$. The linear transformations σ , τ , ϕ_i and ψ_i are computationally cheap as they can be efficiently parallelized and evaluated with $\mathcal{O}(n)$, $\mathcal{O}(n)$, $\mathcal{O}(1)$, $\mathcal{O}(1)$ homomorphic rotations, respectively. Hence, the matrix multiplication method of Jiang et al. has a complexity of $\mathcal{O}(n)$ rotations for two $n \times n$ matrices. This is smaller than previous approaches, such as the naive approach with $\mathcal{O}(n^3)$ or th

Matrix Transpose. Another operation required for RNN training is transpose on matrices as described in Algorithm 2 (Lines 13 and 15). The transpose of a row-packed matrix is straightforward and can be realized with a single linear transform of 2n non-zero diagonals [60] (ξ), hence, it can be evaluated with 2n rotations. This cost can be further reduced to $3\sqrt{n}$ by using the baby-step giant-step (BSGS) algorithm proposed by Halevi and Shoup [48] and later improved by Bossuat et al. [17]. Thus, the cost of a matrix transpose operation is $\mathcal{O}(\sqrt{n})$ for a $n \times n$ matrix.

Multi-dimensional Packing. We propose a novel packing scheme called multi-dimensional packing to optimize the usage of ciphertext slots, which we illustrate in Figure 1b. Given an $n \times n$ matrix and ℓ a divisor of n, we split this matrix into ℓ^2 smaller matrices of size $d \times d$, with $d = \frac{n}{\ell}$. Each of these $d \times d$ -size matrices is stored in a different ciphertext, and we can pack in parallel up to $p = \frac{N}{2} \cdot \frac{\ell^2}{n^2}$ block matrices of size $n \times n$ in a set of ℓ^2 ciphertexts. This packing scheme brings several advantages over the plain row-packing approach by Jiang et al: (i) it enables a more efficient packing of non-squares matrices with a worst case of extra space used reduced from n(n-1) to $n \in \ell$ (ii) it provides a better amortized multiplication complexity as it packs up to $n \in \ell$ matrices (instead of $n \in \ell$) in parallel with $n \in \ell$ 0 complexity for the multiplication, but amortizes to $n \in \ell$ 1 per matrix (instead of $n \in \ell$ 2), (iii) it reduces the complexity of the transpose operation from

 $\mathcal{O}(\sqrt{n})$ to $\mathcal{O}(\sqrt{n/\ell})$ (only the ξ permutation needs to be evaluated on the sub-matrices and permutations between ciphertexts are free), and (iv) it enables more efficient matrix slot manipulations as rows of sub-matrices can be individually moved and/or rotated. We further minimize the number of redundant homomorphic operations by leveraging the techniques used in the *double-hoisting* baby-step giant-step algorithm [17] to evaluate linear transforms and delay ciphertext relinearization, further reducing the complexity. We describe the protocol for multi-dimensional matrix multiplication in Algorithm 3 and the corresponding plaintext operations in Algorithm 5, Appendix C.

RHODE employs the multi-dimensional packing for efficient mini-batch RNN training under encryption. In particular, we distribute the RNN input batch along the "third" dimension (see Figure 1b), by expressing the batch as p parallel matrices (as if computing an ensemble of p parallel RNNs). We can increase the batch size (up to $p*n/\ell$) at no additional cost as it fits into the same ciphertext. To enable further operations, i.e., to make the input batch compatible with the weight matrices, we replicate the latter across the third dimension, so that they are aligned with their parallel slicing of the gradients across the third dimension. These gradients are then aggregated (with $\log(p)$ rotations to perform an inner sum operation), to ensure consistency between the parallel instances. Note that for batches that fit into one ciphertext, our multi-dimensional packing is equivalent to an optimized version (via block-matrices) of Jiang et al.'s [60] approach. However, for bigger matrix dimensions, where the matrix is split over more than one ciphertext, multi-dimensional packing yields better amortized matrix multiplication cost (see Section VI-F).

B. Approximated Neural Network Building Blocks

To compute any non-linear activation or alternative clipping function under CKKS encryption, RHODE relies on polynomial approximations employing the least-squares or Minimax methods. The least-squares method finds the optimal polynomial that minimizes the squared error between the real function and its approximation over an interval, whereas Minimax minimizes the corresponding maximum error. Admittedly, the maximum error with Minimax decreases as the approximation degree (\mathfrak{p}) increases or as the range of the interval shrinks. However, note that with larger \mathfrak{p} , the polynomial evaluation becomes more expensive (with a scale of $O(\log(\mathfrak{p}))$) and smaller interval ranges are not always possible due to the need of accommodating the range of the recurrent neural network outputs. We remark that choosing \mathfrak{p} and the interval of approximations is a non-trivial task under privacy constraints. Yet, these can be determined by synthetic datasets or based on data distribution-based heuristics such as computing the minimum, the maximum, and the mean of feature vector means per dataset [52].

Activation Functions. A neural network is a pipeline of layers composed of neurons on which linear and non-linear transformations (activations) are applied to activate them. Typical activation functions include Sigmoid $(\varphi(x) = \frac{1}{1+e^{-x}})$, ReLU $(\varphi(x) = max(0,x))$, Tanh $(\varphi(x) = \frac{e^x - e^{-x}}{e^x + e^{-x}})$, etc., that are not computable under encryption as they comprise non-linear operations (e.g., comparisons and exponentiations). To overcome this issue, previous works either change the activation functions to other linear or square functions [12], [46], or rely on various approximation techniques employing the least-squares method [40], [110], polynomial splines [75], Legendre [52] or Chebyshev polynomials [86], [52]. For RNNs, the choice of activation function is critical due to exploding gradients problem (i.e., the function should be bounded) and commonly used functions are Tanh and ReLU (that can approximated as SoftPlus, i.e., $\varphi(x) = ln(1+e^x)$ [110]). Thus, similar to prior work, we rely on polynomial approximations employing the least-squares or Minimax methods to enable the execution of these activation functions as we empirically observed that changing them to linear functions decreases the accuracy of RNNs.

Gradient Clipping. As described in Section IV-C, when the weights have a large norm, the gradients accumulated over multiple steps of the BBPT algorithm can grow exponentially; gradient clipping is a well-established technique to mitigate this issue. Thus, in RHODE, the *aggregation server* applies gradient clipping during the Model Update Phase (see Section IV-B). Pascanu et al. [100] propose clipping the gradients based on their infinity-norm, yet applying directly their function under encryption is challenging due to the norm calculation that comprises comparison operations. Thus, inspired from their norm-clipping, we propose a gradient clipping strategy that restricts the infinity-norm of the gradients to a closed interval whose limits are defined by a threshold |m|. To avoid the calculation of the norm under encryption, we apply the following function element-wise to the accumulated gradient vector x:

$$\mathsf{Clip}(x,m) = \begin{cases} -m & x \leq -m \\ x & -m < x < m \\ m & x \geq m \end{cases}$$

Clip(x,m) is a baseline as in practise this function is also difficult to approximate due to its non-smoothness near the clipping interval limits [-m,m]. Therefore, we introduce two softer clipping approximations for clipping gradients. The first one is based on Tanh, which is very similar to Clip except for the clipping interval limits -m and m:

$$\mathsf{TanhClip}(x,\!m)\!=\!m\!*\!tanh\!\left(\frac{x}{m}\right)$$

The second one is based on ReLU, i.e., Clip(x,m) = x + ReLU(-(x+m)) - ReLU(x-m). Since RHODE softly approximates the ReLU function with SoftPlus, SoftClip is defined accordingly as SoftClip(x,m) = x + SoftPlus(-(x+m)) - SoftPlus(x-m), or:

Algorithm 3 Multi-dimensional Matrix Multiplication

Inputs: A, B two $\ell \times \ell$ matrices of ciphertexts, each encrypting a sub-matrix of dimension $(n/\ell) \times (n/\ell)$, the linear transformations σ , τ , ϕ_i and ψ_i (see Section V-A and Figure 1a).

```
Outputs: C \leftarrow A \otimes B
  1: for i=1 \rightarrow \ell do
               for j = 1 \rightarrow \ell do
  2:
  3:
                                                                                                                                                                                                                                                                                  ⊳ Depth 1
                       \mathbf{z} \leftarrow \sigma(\mathbf{B}_{i,j})
                       \mathbf{b}_{i,j} \leftarrow \{\phi_0(\mathbf{z}),...,\phi_{n/\ell-1}(\mathbf{z})\}
  4:
                                                                                                                                                                                                                                                                                  ⊳ Depth 1
  5:
  6: end for
  7: for i=1 \rightarrow \ell do
  8.
               for j = 1 \rightarrow \ell do
                       \mathbf{z} \leftarrow \tau(\mathbf{A}_{i,j})
  9:
                                                                                                                                                                                                                                                                                  Depth 1
 10:
                       \mathbf{a} \leftarrow \{\psi_0(\mathbf{z}), \dots, \psi_{n/\ell-1}(\mathbf{z})\}
                                                                                                                                                                                                                                                                                  ⊳ Depth 1
                       for k=1 \rightarrow \ell do
11:
                              \mathbf{C}_{i,k} \leftarrow \mathbf{C}_{i,k} + \langle \mathbf{a}, \mathbf{b}_{i,j} \rangle
                                                                                                                                                                                                                                                                                  ⊳ Depth 1
12:
13:
               end for
14
15: end for
```

SoftClip
$$(x,m) = x + \ln \frac{1 + e^{-(x+m)}}{1 + e^{(x-m)}}$$

Overall, RHODE enables the approximated execution of both TanhClip and SoftClip with aforementioned polynomial approximations. We evaluate the performance of both clipping approximations and provide the plots of the approximated curves (by using Minimax) and their errors for polynomial degrees of $\mathfrak{p}=5$ and $\mathfrak{p}=15$ in Appendix D. We observe that both functions achieve a similar average error over the approximation interval, yet SoftClip is slightly better than TanhClip for higher degrees (Figures 3c and 3d) in terms of error and behavior around the limits of the approximation interval.

C. Parameter Selection

We now devise guidelines for choosing the parameters that play a vital role for the efficient RNN training execution in RHODE. In particular, we discuss how to select the cryptographic parameters and the sub-matrix dimension $d = n/\ell$ (see Section V-A) that is crucial for the efficiency of the multi-dimensional matrix multiplication (Algorithm 3). RNN-related parameters, e.g., the dimension of the hidden matrix, depend on the learning task and the characteristics of the input data, thus, their configuration is out-of-the-scope of this work.

Cryptographic Parameters. These are linked to the depth of the circuit under evaluation and the desired security level. The circuit depth highly depends on the number of hidden layers and the approximation degree (\mathfrak{p}) of the activation and clipping functions. A higher circuit depth implies a higher number of initial levels \mathcal{L} and Q, for reducing the number of CBootstrap(·) yielding a requirement for bigger cryptographic parameters. To configure the security level, RHODE follows the guidelines of the homomorphic encryption standardization whitepaper for choosing the cyclotomic ring size \mathcal{N} (given the ciphertext modulus Q) [4]. Configuring the cryptographic parameters for the training of neural networks in general is a non-trivial task due to the high number of other parameters that affect their choice, e.g., the number of layers, the polynomial approximation degree, the number of data holders, etc. We refer the reader to [110] for additional details on how to configure the cryptographic parameters based on other neural network learning parameters and to [94] for an overview of the cryptographic parameters.

Choosing d. Recall that the complexity of the matrix multiplication described in Algorithm 3 amortizes to $\mathcal{O}(d)$. In the extreme case where d=1, there are no costly ciphertext operations, except for arithmetic multiplications and additions (no linear transformations are needed). Thus, choosing d=1 minimizes the amortized computational complexity and supports any dimension for the input matrices. However, the memory complexity (in the number of ciphertexts) becomes the number of elements in the input matrices. Since batch sizes are usually in the range $\{64,128,256\}$, it is unlikely that all the $\mathcal{N}/2$ ciphertext slots will be used when setting d=1. In fact, since the number of slots is usually in the range of $\{2^{13},2^{14},2^{15}\}$, this approach would lead to a very low packing density and inefficient memory usage. Instead, we choose a value for d that provides an acceptable trade-off between computational cost and memory complexity. To maximize the packing density, the batch size should be $b=\frac{\mathcal{N}}{2*d}$, thus we can derive that $d=\frac{\mathcal{N}}{2*b}$. Since the batch size can be small due the learning task, we introduce the ciphertext-utilization parameter α that indicates the fraction of the utilized ciphertext slots, to relax the utilization assumption (e.g., $\alpha=1$ and $\alpha=0.5$ indicate full and half utilization, respectively). Given that the batch size cannot be more than maxB and that the ciphertext utilization is at least α we have that:

$$\frac{\mathcal{N} * \alpha}{2 * \mathbf{d}} \le b \le maxB$$

which translates to:

$$d \ge \frac{\mathcal{N} * \alpha}{2*maxB}.$$

For example, in our experiments (see Section VI), we choose $\mathcal{N}=2^{14}$. Thus, for a full ciphertext utilization ($\alpha=1$) at b=256, we have that:

$$d \ge \frac{2^{14}}{2*256} = 32.$$

For a ciphertext utilization of $\alpha = 0.5$, the batch size can be as small as b = 128 at the same d = 32, following a similar calculation.

D. Security Analysis

We demonstrate that RHODE fulfills the data and model confidentiality objectives (Section IV-A) by arguing that a computationally-bounded adversary that controls up to N-1 data holders (i.e., yielding a collusion among N-1 data holders) cannot infer any information about the honest data holder's data or the trained model. We first note that CKKS scheme is IND-CPA secure and its semantic security is based on the hardness of the decisional RLWE problem [26], [80], [74]. We rely on the proofs by Mouchet et al. [94], which show that the MHE cryptographic protocols, i.e., $\mathsf{CKeyGen}(\cdot)$ and $\mathsf{CKeySwitch}(\cdot)$, are secure in a passive-adversary model with up to N-1 collusions as long as the underlying RLWE problem is hard. While their proofs are constructed for the BFV scheme, they generalize to CKKS, since the two schemes rely on the same computational assumptions and hard problem. The security of the collective bootstrapping operation, i.e., $\mathsf{CBootstrap}(\cdot)$, is proven analogously in earlier works employing CKKS -based MHE [40], [110].

Assume that any ciphertext communicated with RHODE is generated using the CKKS cryptosystem parameterized to ensure a post-quantum security level of λ . We rely on the real/ideal world simulation paradigm [73] and consider a real-world simulator $\mathcal S$ that simulates a computationally-bounded adversary corrupting N-1 data holders. During RHODE 's training protocol, the model parameters that are exchanged among data holders at the Aggregate and Model Update Phases are encrypted with the collective public key, while all other phases rely on the collective MHE operations that are proven to be CPA-secure. The result of any computation performed during the Local Computation Phase, following Lemmas 2, 3, and 4 of [26], is a valid encryption under CKKS, thus, achieves a security level of λ . Furthermore, the decryption of any ciphertext requires collaboration among *all* the data holders that participated in CKeyGen(·). To avoid leakage due to two consecutive broadcasts, we rely on an existing countermeasure [94] that re-randomizes any ciphertext before communicating it to the network. As a result, the sequential composition of all cryptographic computations during the training phase of RHODE remains simulatable by $\mathcal S$. Similarly, during RHODE's prediction phase, the data of the querier is encrypted with the collective public key and the prediction result is re-encrypted with the querier's public key; this is the only entity that can decrypt thanks to the simulatable CKeySwitch(·) functionality. Hence, $\mathcal S$ can simulate all of the encryptions communicated during RHODE's training and prediction phase by generating random ciphertexts with equivalent security parameters; the real outputs cannot be distinguished from the ideal ones. Consequently, RHODE protects the confidentiality of the honest data holder's data and the model (following analogous arguments).

VI. SYSTEM EVALUATION

We first theoretically analyze the complexity of RHODE in Section VI-A before empirically evaluating it. We present our experimental setup in Section VI-B and evaluate RHODE's model performance, scalability with different RNN and dataset parameters, runtime performance, and provide various microbenchmarks in Sections VI-C, VI-D, VI-E, and VI-F, respectively.

A. Complexity Analysis

We theoretically analyze RHODE's complexity by taking into account the memory usage per data holder, as well as its communication and computational costs for an Elman network (Algorithm 2). We first derive the total number of ciphertexts required which allows us to estimate the memory usage per data holder. Then, we use the number of ciphertexts to analyze the communication and computation cost of the training process by accounting for the Local Computation, Aggregate, and Model-Update Phases. We exclude the Setup Phase, i.e., the generation of the cryptographic keys (pk, [ek], etc.) and their memory costs from our analysis; this is a one-time phase whose communication cost predominantly depends on the generation of the rotation and relinearization keys (see [94] for details).

Recall that the number of ciphertext slots is $\mathcal{N}/2$, the input size (number of features) is denoted as d, the batch size as b, the hidden dimension as d, the sub-matrix dimension as d, the output size as d, and the number of data holders, local iterations, global iterations, and timesteps as d, d, d, d, d, d, and d, respectively. The maximum size of a ciphertext is denoted by d. To ease the presentation of our complexity analysis we use the following configuration as an example:

Example Configuration: Assume a ring size of $\mathcal{N}=2^{14}$ and ciphertexts with an initial level $\mathcal{L}=10$. Then, assume that d=16, b=256, h=32, d=32, $\kappa=1$ (many-to-one RNN), and o=1 (i.e., a regression task). Finally, assume a degree 7 ($\mathfrak{p}=7$) polynomial approximation of the activation and clipping functions (these are parameters primarily used in our experiments).

Memory Cost. We estimate the memory usage per data holder based on the number of input plaintexts, activation ciphertexts (e.g., \mathbf{h}_t in Algorithm 2), weight ciphertexts (e.g., $\mathbf{U}, \mathbf{V}, \mathbf{W}$), and gradient ciphertexts (e.g., $\nabla \mathbf{U}, \nabla \mathbf{W}, \nabla \mathbf{V}$). We denote the number of plaintexts used to pack a vector/matrix a as |a|, and the number of ciphertexts with bold-face a. We first calculate the number of matrix rows/columns that

each ciphertext can pack. Since we rely on row-based packing, the number of matrix rows per ciphertext is $\left\lfloor \frac{\mathcal{N}}{2*\mathrm{cl}} \right\rfloor$ and the number of columns per ciphertext is d , for any matrix size. As we split the input batch over the third dimension (i.e., the size of a ciphertext), the number of sub-matrix rows per ciphertext is $\left\lceil \frac{b}{(\mathcal{N}/2)/\mathrm{d}} \right\rceil = \left\lceil \frac{2*\mathrm{d}*b}{\mathcal{N}} \right\rceil$ and the number of sub-matrix columns is $\left\lceil \frac{c}{\mathrm{d}} \right\rceil$, for any column of size c. These allow us to derive the total number of plaintexts required for the input batch and **activation** ciphertexts as:

$$|x_t| = \left\lceil \frac{2*d*b}{\mathcal{N}} \right\rceil * \left\lceil \frac{d}{d} \right\rceil \quad \text{(input plaintexts)}$$

$$|\mathbf{z}_t| = |\mathbf{h}_t| = \left\lceil \frac{2*d*b}{\mathcal{N}} \right\rceil * \left\lceil \frac{h}{d} \right\rceil \quad \text{(hidden ciphertexts)}$$

$$|\mathbf{p}_t| = \left\lceil \frac{2*d*b}{\mathcal{N}} \right\rceil * \left\lceil \frac{o}{d} \right\rceil \quad \text{(output ciphertexts)}$$

As we replicate the weight matrices for the sub-matrix operations (see Section V-A), for an $n \times m$ weight matrix, the number of sub-matrix rows and columns per weight ciphertext is $\left\lceil \frac{n}{\mathrm{d}} \right\rceil$ and $\left\lceil \frac{m}{\mathrm{d}} \right\rceil$, respectively. Therefore, the total number of ciphertexts for the **weight** matrices are:

$$\begin{split} |\mathbf{U}| &= \left\lceil \frac{d}{\mathrm{d}} \right\rceil * \left\lceil \frac{h}{\mathrm{d}} \right] \quad \text{(input-weight ciphertexts)} \\ |\mathbf{W}| &= \left\lceil \frac{h}{\mathrm{d}} \right\rceil * \left\lceil \frac{h}{\mathrm{d}} \right\rceil \quad \text{(hidden-weight ciphertexts)} \\ |\mathbf{V}| &= \left\lceil \frac{h}{\mathrm{d}} \right\rceil * \left\lceil \frac{o}{\mathrm{d}} \right\rceil \quad \text{(output-weight ciphertexts)} \end{split}$$

Finally, the number of gradient ciphertexts per weight matrix is the same as the number of ciphertexts for the respective activation or weight matrix. The number of plaintexts and ciphertexts sets an upper bound to the memory cost per data holder, per timestep execution. Yet, not all computed values need to be stored during the training. For example, when the activation function is Tanh, $dh \odot \varphi'(\mathbf{z}_t)$ (Line 14, Algorithm 2) is equivalent to $dh \odot (1 - \mathbf{h}_t^2)$ as the derivative of Tanh(x) is $1 - Tanh^2(x)$. Thus, \mathbf{z}_t is computed on-the-fly in the forward pass, and then discarded as it is not used in the backward one. For the Example Configuration, RHODE requires only one ciphertext for each activation, weight, and gradient matrix.

Communication Cost. The number of ciphertexts storing the weight matrices has a direct impact on RHODE's communication cost. During RNN training, communication among the data holders is triggered by: (a) the collective bootstrapping (CBootstrap(\cdot)) operation to refresh the ciphertexts, and (b) the federated learning (FL) workflow, where data holders aggregate their locally computed gradients (i.e., Aggregate Phase) before the *aggregation server* updates the global model and broadcasts it (i.e., Model-Update Phase).

Collective Bootstrapping. The total number of bootstrapping operations depends on both the learning and the cryptographic parameters. For instance, the approximation degree of the activation or clipping functions (\mathfrak{p}) and the polynomial ring dimension (\mathcal{N}) have a direct effect on the depth of the circuit and thus, the number of bootstraps. We refer the reader to [110] for the detailed estimation of the number of bootstraps depending on the learning and the cryptographic parameters. For the Example Configuration, RHODE bootstraps \mathbf{h}_t (Line 5) and \mathbf{dz} (Line 14) in the forward pass of each local timestep iteration (Algorithm 2). After the execution of all timesteps, the intermediate term $\mathbf{I} = \mathbf{h}_t \otimes \mathbf{dy}$ (Line 16) in the backward pass is bootstrapped in the output stage, i.e., RHODE executes one bootstrap for a one/many-to-one RNN structure and κ bootstraps for one/many-to-many structures on \mathbf{I} where $|\mathbf{I}| = |\mathbf{dz}|$. RHODE also bootstraps the weight ciphertexts \mathbf{U} , \mathbf{V} , and \mathbf{W} , after the Model-Update Phase to refresh them before the next training round. Thus, the communication cost due to the collective bootstrapping operation (BS_c) is:

$$BS_c < e(|\mathbf{U}| + |\mathbf{W}| + |\mathbf{V}| + l|\mathbf{I}|\kappa + Tl(|\mathbf{ht}| + |\mathbf{dz}|))(N-1)s.$$

Recall that s sets an upper bound for the sent/received messages; the communication cost of the bootstrapping is lower in practise. For the Example Configuration $BS_c = (4+2T)(N-1)s$ per local iteration.

FL Workflow. During a global training iteration, the data holders collectively aggregate their locally computed gradients (i.e., ∇U , ∇W , ∇V , see Line 8, Algorithm 1) and the aggregation server updates the global model and broadcasts its weights (i.e., U, W, V, Line 4, Algorithm 1). In RHODE, data holders are organized in a tree-structured network topology, thus, they collectively aggregate their gradients by sending them to their parent in the tree. Then, the aggregation server broadcasts the updated weights down the tree. Given that this communication is incurred for every global iteration, the total communication cost (FL_c) is:

$$FL_c = (|\nabla \mathbf{U}| + |\nabla \mathbf{W}| + |\nabla \mathbf{V}| + |\mathbf{U}| + |\mathbf{W}| + |\mathbf{V}|)e(N-1)s.$$

Computational Cost. We estimate RHODE's computational cost per data holder and per local iteration taking into consideration the dominating terms, i.e., the number of CBootstrap(·) operations (which are ~ 2 orders of magnitude slower than a homomorphic

addition/multiplication), the degree \mathfrak{p} , and the cost of the linear transformations (i.e., σ, τ, ψ_i and ϕ_i) required for the matrix multiplication. Note that bootstrapping a ciphertext at a level \mathcal{L}_c (with an initial level \mathcal{L}) has a complexity of $C(BS) = \mathcal{N}\log_2(\mathcal{N})(\mathcal{L}+1) + \mathcal{N}\log_2(\mathcal{N})(\mathcal{L}_c+1)$, homomorphic rotations have a complexity of $C(R) = \mathcal{O}(\mathcal{N}\log_2(\mathcal{N})\mathcal{L}_c^2)$, and ciphertext-ciphertext multiplications have a complexity of $C(M) = 4N(\mathcal{L}_c+1) + C(R)$ [110].

The degree (\mathfrak{p}) of the polynomial approximation affects the depth of the circuit required for an activation function; computing φ (or its derivative φ') consumes $\lceil \log_2(\mathfrak{p}) \rceil$ ($\lceil \log_2(\mathfrak{p}-1) \rceil$, respectively) levels. Thus, using a higher \mathfrak{p} for polynomial approximation has two consequences to the computational cost: (i) it increases the depth of the circuit, hence the number of bootstraps, and (ii) results in more homomorphic multiplications. As discussed in Section V-A, the multi-dimensional matrix multiplication (Algorithm 3) consumes 3 levels and yields an amortized cost of $\mathcal{O}(d)$ rotations per matrix (depending on d, see Section V-C). The Example Configuration requires 6 matrix multiplications per timestep (8 for the output-stage timestep due to the multiplications with \mathbf{V} and $\mathbf{V}^{\mathbf{T}}$ which adds a constant factor to the complexity), thus yielding a computation complexity of $\mathcal{O}(6Td)$ rotations for a local iteration of T timesteps and per ciphertext. Note that the matrix multiplication complexity predominantly comes from the linear transformations; the rest of the algorithm comprises only multiplications and additions, which are negligible in comparison. RHODE's RNN training protocol requires several multiplications with the weight matrices ($\mathbf{W}, \mathbf{U}, \mathbf{V}$) and their transposes ($\mathbf{V}^T, \mathbf{W}^T$). As these matrices are not updated through the local iteration of each timestep, we can pre-compute their linear transformations at the beginning of each iteration and re-use them for all timesteps. For the Example Configuration, this reduces the cost to $\mathcal{O}(6\mathrm{d})$ per local iteration, at a memory cost of $\times d$ per matrix.

B. Experimental Setup

We now present our implementation details and the datasets used for RHODE's model performance evaluation. We describe the data distribution, the RNN configuration, and the security parameters.

Implementation Details. We implement RHODE in Go [3] and employ the Lattigo [86] lattice-based HE library for the multiparty homomorphic operations. We rely on Onet [2] to build a decentralized system where the data holders communicate over TCP with secure channels (TLS) and Mininet [87] to emulate a virtual network. Our experiments are performed on 10 Linux servers with Intel Xeon E5-2680 v3 CPUs running at 2.5GHz with 24 threads on 12 cores and 256 GB RAM emulating a virtual network with an average network delay of 20ms and 1Gbps bandwidth.

Datasets and Preprocessing. We employ the Hourly Energy Consumption (HEC) [56] and Stock Prices (Stock) datasets [119] for time-series forecasting tasks. HEC contains the historical hourly energy consumption (in MegaWatts) of several electricity distribution companies (one file per company) during a specific time period [56]. A common task performed on this dataset is to use early sequences of energy consumption values and predict the future value for sequences of length T. The total number of samples in this dataset is over 1M, and we use varying number of samples for our experiments. The **Stock** dataset contains historical daily stock prices and statistics for 10 companies, such as Apple and Twitter, from varying dates. This dataset was collected from the Yahoo! Finance website [119]. The task on this dataset is to predict the average open-high-low-closing (OHLC) price for the next day, given the OHLC of the previous T days. The total number of samples (across all 10 companies) is over 39K. For each experimental setting, we split the dataset into training (80%) and test (20%) sets. We also apply Min-Max scaling on the data to minimize the risk of explosion on the approximated activation functions. More details about these datasets can be found in Appendix A. For the experiments analyzing RHODE's scalability and microbenchmarks, we use synthetic datasets.

Dataset Distribution. For the model performance experiments (Section VI-C), we split the data among N=10 data holders and evaluate two different settings: (i) Even (E) distribution, where we uniformly distribute the dataset samples to the N data holders, and (ii) Imbalanced (I) distribution where we simulate a heterogeneous setting, with each data holder having one dataset file (see Appendix A), e.g., for the Stock dataset, a data holder might be Apple Inc. contributing the stock prices of only Apple. We annotate the results per setting as "DatasetName-TypeT" where Type denotes the type of the data distribution, and T the sequence length T, e.g., HEC-I10, denotes imbalanced data distribution and a sequence length of T=10 on the HEC dataset. RNN Configuration. For the model performance experiments (Section VI-C), we use a many-to-one RNN structure (commonly employed for time-series forecasting based on step-by-step predictions), a local batch size of b=256, a hidden dimension of h=32, and varying timesteps T=[5,10,20]. The number of features for HEC is d=6 and for Stock is d=1 (see Appendix A). For all experiments per dataset, we use the same RNN structure and learning parameters: We use a learning rate of $\eta=0.1$, we clip the gradients using SoftClip(x,m) with a clipping threshold of |m|=5 and approximated with a $\mathfrak{p}=7$ polynomial in the interval [-60,60] as a result of a preliminary evaluations on the datasets. Each data holder performs one local iteration and we train the RNN for 300 and 1,000 global iterations, for the Stock and HEC datasets, respectively. To expedite the model performance experiments (Section VI-C), we simulate RHODE's fully-encrypted training pipeline in cleartext by using the approximated activation and clipping functions, and a fixed-precision.

Security Parameters. Unless otherwise stated, we set the degree of the cyclotomic polynomial to $\mathcal{N}=2^{14}$ and the modulus of the keys to $Q \approx 2^{438}$. These parameters yield 128-bit security according to the homomorphic encryption standard [10]. We set the plaintext scale to 2^{31} , and the initial ciphertext level is $\mathcal{L}=9$.

C. Model Performance

Table I shows RHODE's model performance results on the HEC and Stock datasets in various settings. For each setting, we report the mean squared error (MAE) and the coefficient of determination (\mathbb{R}^2) averaged over all files. For comparison purposes, the table displays the

Dataset		Model Performa	$nce (MAE \mid R^2)$)
	L	С	FL	RHODE
Stock-E5	0.023 0.966	0.008 0.996	0.020 0.982	0.017 0.987
Stock-I5	0.024 0.976	0.008 0.996	0.012 0.992	0.012 0.992
HEC-E10	0.066 0.749	0.014 0.987	0.024 0.965	0.026 0.957
HEC-I10	0.081 0.625	0.014 0.987	0.025 0.962	0.027 0.955
HEC-E20	0.066 0.749	0.014 0.986	0.024 0.964	0.026 0.957
HEC-I20	0.081 0.626	0.014 0.986	0.025 0.962	0.027 0.954

TABLE I: RHODE's model performance in various settings where the Stock and HEC datasets are split among N=10 data holders. The performance is compared to three baselines: local training without collaboration (\mathbf{L}), centralized (\mathbf{C}), and federated learning (\mathbf{FL}).

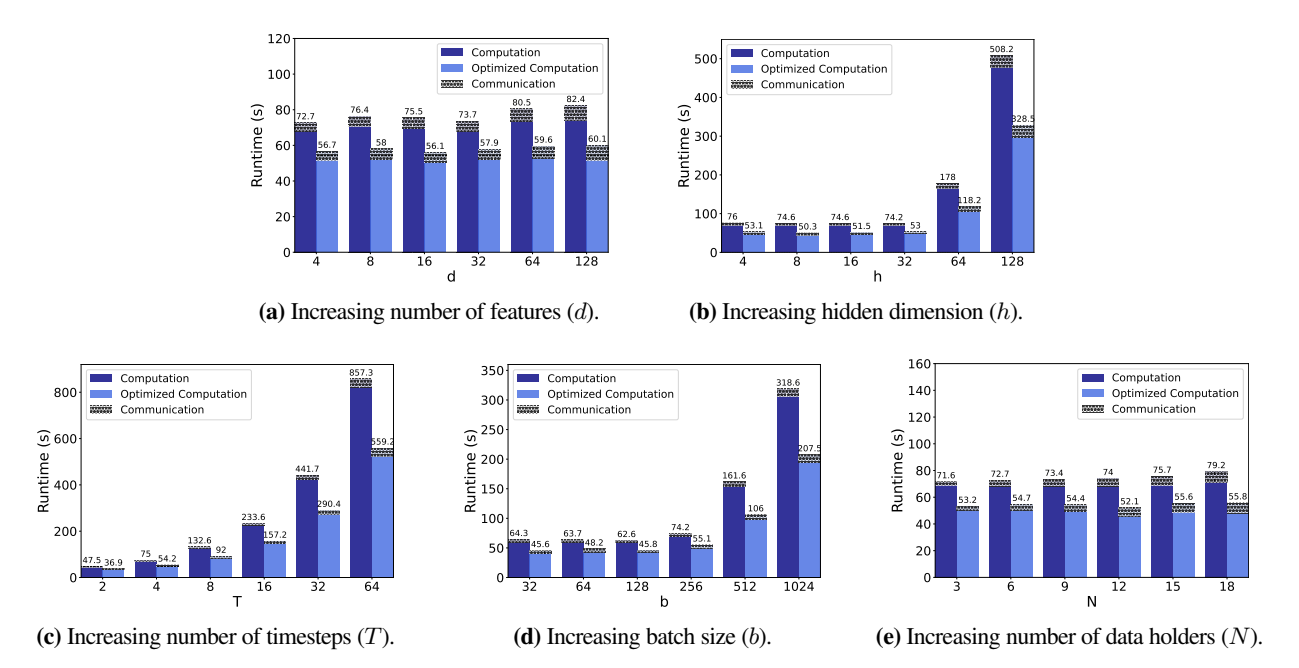


Figure 2: RHODE's training execution times for computation and communication for one global iteration with increasing (a) number of features, (b) hidden dimension, (c) timesteps, (d) batch size, and (e) number of data holders. The default network parameters are h = d = T = 4, b = 256, d = 32 (we vary one of them in the corresponding experiment while keeping the others fixed), and the number of data holders is N = 10.

MAE and R^2 of three baselines: (a) **L** stands for local training, where each data holder trains its own local model with the original network, i.e., without taking advantage of the other data holders' inputs, (b) **C** stands for centralized training, where all the data is collected to a central server and trained with the original network (original activation functions and clipping), and (c) **FL** stands for a **FL** approach, where the data is distributed among 10 data holders and the learning is performed without any privacy mechanism. The last column shows the performance of Rhode for privacy-preserving **FL** training. The baseline column **L** shows the performance gain of collaborative training (note that we report the MAE and R^2 averaged across the 10 data holders). Whereas, the baselines **C** and **FL** enable us to evaluate Rhode's performance loss due to collective learning, the approximation of the activation/clipping functions, and the encryption.

In all settings, we observe that RHODE achieves a model performance comparable to non-private baselines, e.g., at most 0.03 difference in R^2 -score compared to a centralized solution, and at most 0.01 from a federated learning (FL) approach. We also observe that there is always a performance gain, compared to \mathbf{L} . For instance, the gain in terms of R^2 -score for the Stock dataset is between 0.01-0.02, whereas it is between 0.21-0.33 for the more complex HEC dataset. More importantly, for an imbalanced distribution, i.e., HEC-I10 or HEC-I20, the gain from collaborative learning is more substantial (~ 0.33 increase in R^2 -score). We observe a similar trend on the MAE, justifying the use of privacy-preserving collaborative learning over local training without collaboration.

D. Scalability Analysis

We use synthetic datasets on which we vary the number of features (d), the hidden dimension (h), the timesteps (T), the batch size (b), and the data holders (N) for a global iteration. Our default network parameters are h=d=T=4, b=256, and d=32, the number of data

providers is N = 10, and we vary the parameter under analysis. The calculated runtime includes average per-data holder Local Computation, as well as the Aggregate, and Model-Update Phases. Figure 2 shows the time spent by RHODE (and its optimized version with pre-generated linear transforms, described in Section VI-A) on computation and on communication during a global iteration. The communication indicates the total time spent for the collective bootstrapping operations (CBootstrap(\cdot)) and the collective aggregation. Overall, we observe that

	Runtime (s)					
Structure (b,d,h,T)	Training	Training (Opt)	Prediction	Prediction (Opt)		
(256, 4, 32, 4)	72.65	56.68	27.61	18.10		
(256, 32, 32, 4)	73.66	57.94	28.06	18.55		
(256, 64, 32, 4)	80.48	59.63	31.04	20.53		
(256, 4, 16, 4)	74.56	51.45	29.28	15.50		
(256, 4, 32, 4)	74.19	53.04	71.92	16.31		
(256, 4, 64, 4)	178.01	118.17	225.34	56.41		

TABLE II: RHODE's training and prediction runtime (including communication) for several many-to-one RNN architectures with N=10 data holders. Training runtimes are for one global iteration and Prediction runtimes are for oblivious predictions (both the data and the model are encrypted) on 256 samples. Opt stands for optimized execution.

the optimized computation is always more efficient in terms of runtime at a memory cost of $32 \times$ more ciphertexts per weight matrix (see Section VI-A). Moreover, Figures 2a, 2b and 2d demonstrate that RHODE's computation time remains constant, with increasing the respective parameters $\{d,h,b\}$ when d,h,b < d. This is due to the SIMD operation support by the HE scheme; as for these settings the number of matrix entries fit into one ciphertext, RHODE enables processing larger batches (more samples) or larger networks at zero additional cost.

In more detail, Figure 2a shows that RHODE scales sub-linearly with d and that the effect of increasing d is almost negligible in runtime. This is because each data holder's data remains in clear form through the training and the plaintext operations are negligible, compared to ciphertext ones. Increasing d has a direct effect on the matrix multiplication $(x_t \times \mathbf{U})$ of the first layer, as x_t is a plaintext whose size depends on d. As a result, the effect of increasing d is not observable, as the ciphertext multiplications, i.e., $\mathbf{h_{t-1}} \times \mathbf{W}$, dominate the runtime. The communication overhead also scales sub-linearly; increasing d increases the number of ciphertexts to be bootstrapped (see Section VI-A). Figure 2b shows that RHODE scales sub-quadratically, with increasing d when d = 32; while increasing d quadratically increases the number of ciphertexts for the weight matrix d, this affects the runtime of a few matrix multiplications only (see Section VI-A). This trend holds also for the communication due to an increased number of ciphertexts that are bootstrapped by the aggregation server for d. Figures 2c and 2d demonstrate that RHODE's runtime scales linearly with increasing d or d; this is due to the sequential operations over the d timesteps or the linear increase in the number of ciphertexts processed when increasing d. Finally, Figure 2e shows that RHODE's local computation time remains constant with increasing number of data holders, as the local computations per data holder are performed in parallel. The communication overhead increases linearly with increasing d, as more data holders are involved in the interactive protocols, i.e., the CBootstrap(·) and the Aggregate Phase.

E. Runtime Performance

Table II displays RHODE's training and prediction runtimes (for the original and optimized implementations) for various many-to-one RNN architectures with N=10 data holders. The Training runtime is for one global iteration (including the communication for CBootstrap(·) and Aggregate Phase). The Prediction runtime is for oblivious predictions (both data and model are encrypted) on a batch of 256 samples (including the communication for CKeySwitch(·) that changes the key of the prediction result to the querier's public key). The results of this table can be used along with the scalability results of Section VI-D to estimate RHODE's total training runtime for various RNN structures. For instance, RHODE can process 256K samples split among 10 data holders with an RNN with b=256, d=4, h=32, T=4 (first table row), over 100 global iterations, in ~ 1.5 (~ 2) hours with its optimized (non-optimized, respectively) implementation. Moreover, as the Prediction runtime is calculated for a batch of 256 samples, RHODE yields a prediction throughput of ~ 14.43 (~ 9.31) samples per second with its optimized (non-optimized, respectively) implementation, for an RNN with the same structure.

F. Microbenchmarks

Multi-dimensional Packing vs. [60]. We compare our packing scheme with Jiang et al.'s [60] approach in Tables III (timings) and IV (memory). We report the total and amortized time (or throughput) by executing #M multiplications of $n \times n$ -size matrices in parallel. We observe that if n=d, then both approaches perform identically; this is expected since Jiang et al.'s approach is a special case of our multi-dimensional packing with only one ciphertext. For n>d the multi-dimensional packing requires more time to complete the multiplications but achieves a better amortized time than Jiang et al's approach. Due to memory limitations, we were not able to benchmark Jiang et al.'s approach for n=256 and n=512. This is a consequence of each method's memory requirements (see Table IV). The memory overhead arises particularly from the ring dimension (\mathcal{N}) , the number of ciphertexts, and the size of the evaluation keys. The first row of Table IV shows that, with Jiang et al.'s method,

 $\mathcal N$ scales quadratically with n compared to ours that scales similarly with d (or with the closest power of two above n^2 or d^2 , respectively). In other words, for larger matrices (e.g., when multiplying two 128×128 matrices), Jiang et al.'s approach requires increasing $\mathcal N$ (as the matrix does not fit into one ciphertext), whereas our approach increases only the number of ciphertexts for a fixed d (see the second row of Table III). However, Jiang et al.'s approach also significantly impacts the size of the evaluation keys. Indeed, as in their approach $\mathcal N$ scales with $\mathcal O(n^2)$, increasing n has the side effect of increasing the evaluation keys' size (see third row of Table III). Recall that Jiang et al.'s method also requires $\mathcal O(n)$ evaluation keys to perform the multiplication, thus resulting in an overall $\mathcal O(n^3)$ memory complexity. In contrast, our approach provides a better memory complexity, with only $\mathcal O(d^3)$ that is $\mathcal O(1)$ for a fixed d. In conclusion, our multi-dimensional packing is at least equivalent to Jiang et al.'s [60] and can be configured to provide a better throughput for settings with large batch sizes or hidden dimensions such that the inputs/weights do not fit into one ciphertext. It also uses a constant memory for the evaluation keys, regardless of the matrix dimension n; this enables the multiplication between large matrices, without the need for larger cryptographic parameters or the re-generation of the evaluation keys.

Dimension	Jiang et al. [60]			Multi-dimensional (d = 32)		
$n \times n$	Total Amortized (s)	#M	\mathcal{N}	Total Amortized (s)	#M	\mathcal{N}
32×32	0.43 0.05	8	14	0.43 0.05	8	14
64×64	0.82 0.41	2	14	1.70 0.21	8	14
$128\!\times\!128$	2.86 2.86	1	15	7.16 0.89	8	14
$256\!\times\!256$	NA	1	16	30.6 3.82	8	14
512×512	NA	1	19	79.17 9.89	8	14

TABLE III: Comparison between our multi-dimensional packing and Jiang et al.'s [60] approach. We report the total and amortized runtime per matrix for the multiplication of #M matrices of size $n \times n$. $\mathcal N$ is the ring size, and NA indicates that the memory was insufficient to carry out the evaluation.

	Jiang et al. [60]	Multi-dimensional
\mathcal{N}	$\mathcal{O}(n^2)$	$\mathcal{O}(\mathrm{d}^2)$
#Ciphertexts	$\mathcal{O}(1)$	$\mathcal{O}(n^2/\mathring{\mathrm{d}}^2)$
Evaluation Keys (Size)	$\mathcal{O}(n^3)$	$\mathcal{O}(\mathrm{d}^3)$

TABLE IV: Comparison of the memory complexity between our multi-dimensional packing and Jiang et al.'s [60] approach, with respect to the matrix dimension n and sub-matrix dimension d.

RNN Structure. We evaluate RHODE's performance for different RNN structures including many-to-one and many-to-many. Table V depicts the results of microbenchmarks for the forward and backward passes per timestep without bootstrapping and without optimization for different RNN structures. FP, BP, FP- t_o , and BP- t_o , stands for the forward pass, the backward pass of the output-stage timestep, and the backward pass of the output-stage timestep, respectively. The columns 'FP Total' and 'BP Total' show the total time required for the execution of the FP and BP, respectively. For example, the first row is a many-to-one RNN structure with T=6 and $\kappa=1$. This means that the FP is calculated for 6-1=5 timesteps and FP- t_o is calculated once. Similarly, for the second row with T=6 and $\kappa=2$, the FP is calculated for 6-2=4 timesteps, whereas FP- t_o is calculated for 2. There is no FP and BP for the last row as $T=\kappa=6$. Overall, Table V shows that the forward and backward pass calculations of the output-stage timestep (FP- t_o , BP- t_o) are more costly than the usual FP and BP timesteps ($1.7\times$). This is due to the extra multiplication required in the FP for calculating the prediction (Line 6, Algorithm 2), and the extra subtraction and multiplication during the BP (Lines 12-13, Algorithm 2) for the output error calculation. Recall that Algorithm 2 is presented for a many-to-many RNN structure with $\kappa=T$ outputs. The computations of Lines 6, 12, and 13, are executed κ times for other structures with $\kappa\neq T$. Consequently, many-to-many RNN structures are more expensive, and the increase in the runtime depends on κ .

	Runtime (s)					
Structure (b,d,h,T,o,κ)	FP	$\operatorname{FP-}t_o$	BP	BP- t_o	FP Total	BP Total
(256, 64, 32, 6, 1, 1) (256, 64, 32, 6, 1, 2) (256, 64, 32, 6, 1, 4) (256, 64, 32, 6, 1, 6)	4.36 4.42 4.32	7.44 7.39 7.47 7.38	7.60 7.62 7.55	11.55 11.47 11.59 11.42	29.24 32.46 38.52 44.28	49.55 53.42 61.46 68.52

TABLE V: Microbenchmarks for the forward and backward passes per timestep for various RNN structures without optimization. FP and BP stands for the forward pass and the backward pass, respectively. t_o represents the timestep at the output stage.

VII. CONCLUSION

In this work, we presented RHODE, a novel system that enables privacy-preserving training of and predictions on Recurrent Neural Networks (RNNs) in a federated learning setting. Building on multi-party homomorphic encryption (MHE), RHODE preserves the confidentiality of the training data, the model, and the prediction data, under a passive adversary model with collusions of up to N-1 parties. By leveraging on a novel multi-dimensional packing scheme and polynomial approximations for clipping and activation functions, RHODE enables efficient mini-batch training and addresses the problem of exploding (or vanishing) gradients that is inherent in RNNs. RHODE scales sub-linearly with the number of features and the number of data holders, linearly with the number of timesteps and the batch size, and its accuracy is on par with non-secure centralized and decentralized solutions. To the best of our knowledge, RHODE is the first system providing the building blocks for federated training of RNNs and its variants under encryption. As future work, we plan to evaluate RHODE on sequential data types other than time-series and on more complex recurrent neural network architectures.

REFERENCES

- [1] Centers for Medicare & Medicaid Services. The Health Insurance Portability and Accountability Act of 1996 (HIPAA). https://www.cms.gov/Regulations-and-Guidance/Administrative-Simplification/HIPAA-ACA/PrivacyandSecurityInformation. (Accessed: 2022-01-06).
- [2] Cothority network library. https://github.com/dedis/onet. (Accessed: 2022-01-06).
- [3] Go Programming Language. https://golang.org. (Accessed: 2022-01-06).
- [4] Homomorphic Encryption Standardization. https://homomorphicencryption.org/standard/. (Accessed: 2022-01-06).
- [5] The EU General Data Protection Regulation. https://gdpr-info.eu/. (Accessed: 2022-01-06).
- [6] Cheetah: Lean and fast secure Two-Party deep neural network inference. In 31st USENIX Security Symposium (USENIX Security 22), Aug. 2022.
- [7] M. Abadi, A. Chu, I. Goodfellow, H. B. McMahan, I. Mironov, K. Talwar, and L. Zhang. Deep learning with differential privacy. In ACM CCS, 2016.
- [8] N. Agrawal, A. S. Shamsabadi, M. J. Kusner, and A. Gascón. QUOTIENT: Two-party secure neural network training and prediction. ACM CCS, 2019.
- [9] A. Akavia, H. Shaul, M. Weiss, and Z. Yakhini. Linear-regression on packed encrypted data in the two-server model. In ACM WAHC, 2019.
- [10] M. Albrecht et al. Homomorphic Encryption Security Standard. Technical report, HomomorphicEncryption.org, 2018.
- [11] G. Asharov, A. Jain, A. López-Alt, E. Tromer, V. Vaikuntanathan, and D. Wichs. Multiparty computation with low communication, computation and interaction via threshold FHE. In D. Pointcheval and T. Johansson, editors, *Advances in Cryptology EUROCRYPT 2012*, pages 483–501, Berlin, Heidelberg, 2012. Springer Berlin Heidelberg.
- [12] M. Bakshi and M. Last. Cryptornn privacy-preserving recurrent neural networks using homomorphic encryption. In S. Dolev, V. Kolesnikov, S. Lodha, and G. Weiss, editors, *Cyber Security Cryptography and Machine Learning*, pages 245–253, Cham, 2020. Springer International Publishing.
- [13] M. Barni, P. Failla, R. Lazzeretti, A.-R. Sadeghi, and T. Schneider. Privacy-preserving ecg classification with branching programs and neural networks. IEEE Transactions on Information Forensics and Security, 6(2):452–468, 2011.
- [14] Y. Bengio, P. Simard, and P. Frasconi. Learning long-term dependencies with gradient descent is difficult. *IEEE Transactions on Neural Networks*, 5(2):157–166, 1994.
- [15] F. Boemer, A. Costache, R. Cammarota, and C. Wierzynski. ngraph-he2: A high-throughput framework for neural network inference on encrypted data. In *ACM WAHC*, 2019.
- [16] D. Bogdanov, L. Kamm, S. Laur, and V. Sokk. Rmind: a tool for cryptographically secure statistical analysis. IEEE TDSC, 15(3):481–495, 2018.
- [17] J.-P. Bossuat, C. Mouchet, J. Troncoso-Pastoriza, and J.-P. Hubaux. Efficient bootstrapping for approximate homomorphic encryption with non-sparse keys. In A. Canteaut and F.-X. Standaert, editors, *Advances in Cryptology EUROCRYPT 2021*, pages 587–617, Cham, 2021. Springer International Publishing.
- [18] A. Boulemtafes, A. Derhab, and Y. Challal. A review of privacy-preserving techniques for deep learning. Neurocomputing, 384:21–45, 2020.
- [19] J. W. S. Brown, O. Ohrimenko, and R. Tamassia. Haze: Privacy-preserving real-time traffic statistics. In Proceedings of the 21st ACM SIGSPATIAL International Conference on Advances in Geographic Information Systems, SIGSPATIAL'13, page 540–543, New York, NY, USA, 2013. Association for Computing Machinery.
- [20] E. Buchmann, K. Böhm, T. Burghardt, and S. Kessler. Re-identification of smart meter data. Personal and Ubiquitous Computing, 17(4):653-662, Apr 2013.
- [21] M. Byali, H. Chaudhari, A. Patra, and A. Suresh. FLASH: Fast and robust framework for privacy-preserving machine learning. PETS, 2020.
- [22] S. Chandar, C. Sankar, E. Vorontsov, S. E. Kahou, and Y. Bengio. Towards non-saturating recurrent units for modelling long-term dependencies. In *Proceedings of the Thirty-Third AAAI Conference on Artificial Intelligence and Thirty-First Innovative Applications of Artificial Intelligence Conference and Ninth AAAI Symposium on Educational Advances in Artificial Intelligence*, AAAI 19/IAAI 19/EAAI 19. AAAI Press, 2019.
- [23] H. Chaudhari, R. Rachuri, and A. Suresh. Trident: Efficient 4pc framework for privacy preserving machine learning. In NDSS, 2020.
- [24] M. Chen, R. Mathews, T. Ouyang, and F. Beaufays. Federated learning of out-of-vocabulary words. CoRR, abs/1903.10635, 2019.
- [25] T. Chen and S. Zhong. Privacy-preserving backpropagation neural network learning. IEEE Transactions on Neural Networks, 20(10):1554–1564, Oct 2009.
- [26] J. H. Cheon, A. Kim, M. Kim, and Y. Song. Homomorphic encryption for arithmetic of approximate numbers. In ASIACRYPT, 2017.
- [27] H. Cho, D. Wu, and B. Berger. Secure genome-wide association analysis using multiparty computation. Nature Biotechnology, 36:547–551, 2018.
- [28] K. Cho, B. van Merriënboer, D. Bahdanau, and Y. Bengio. On the properties of neural machine translation: Encoder–decoder approaches. In *Proceedings of SSST-8, Eighth Workshop on Syntax, Semantics and Structure in Statistical Translation*, pages 103–111. Association for Computational Linguistics, Oct. 2014.
- [29] C. A. Choquette-Choo, N. Dullerud, A. Dziedzic, Y. Zhang, S. Jha, N. Papernot, and X. Wang. Capc learning: Confidential and private collaborative learning. In 9th International Conference on Learning Representations, ICLR 2021, Virtual Event, Austria, May 3-7, 2021, 2021.
- [30] C.-T. Chu, S. K. Kim, Y.-A. Lin, Y. yu, G. Bradski, A. Ng, and K. Olukotun. Map-reduce for machine learning on multicore. In NIPS, 2006.
- [31] E. Dauterman, M. Rathee, R. Popa, and I. Stoica. Waldo: A private time-series database from function secret sharing. In 2022 2022 IEEE Symposium on Security and Privacy (SP) (SP), pages 668–686, Los Alamitos, CA, USA, may 2022. IEEE Computer Society.
- [32] J. Deng, Y. Wang, J. Li, C. Wang, C. Shang, H. Liu, S. Rajasekaran, and C. Ding. TAG: Gradient attack on transformer-based language models. In *EMNLP*, pages 3600–3610, 2021.
- [33] R. Dey and F. M. Salem. Gate-variants of gated recurrent unit (gru) neural networks. In 2017 IEEE 60th International Midwest Symposium on Circuits and Systems (MWSCAS), pages 1597–1600, 2017.
- [34] D. I. Dimitrov, M. Balunović, N. Jovanović, and M. Vechev. Lamp: Extracting text from gradients with language model priors. CoRR, abs/2202.08827, 2022.
- [35] J. L. Elman. Finding structure in time. Cognitive Science, 14(2):179–211, 1990.
- [36] M. N. Fekri, K. Grolinger, and S. Mir. Distributed load forecasting using smart meter data: Federated learning with recurrent neural networks. *International Journal of Electrical Power & Energy Systems*, 137:107669, 2022.
- [37] B. Feng, Q. Lou, L. Jiang, and G. C. Fox. Cryptogru: Low latency privacy-preserving text analysis with gru. *CoRR*, abs/2010.11796, 2021.
- [38] Q. Feng, D. He, Z. Liu, H. Wang, and K.-K. R. Choo. Securenlp: A system for multi-party privacy-preserving natural language processing. IEEE Transactions on Information Forensics and Security, 15:3709–3721, 2020.
- [39] M. Franklin and S. Haber. Joint encryption and message-efficient secure computation. Journal of Cryptology, 9(4):217–232, Sep 1996.
- [40] D. Froelicher, J. R. Troncoso-Pastoriza, A. Pyrgelis, S. Sav, J. S. Sousa, J.-P. Bossuat, and J.-P. Hubaux. Scalable privacy-preserving distributed learning. PETS, 2021.

- [41] D. Froelicher, J. R. Troncoso-Pastoriza, J. L. Raisaro, M. A. Cuendet, J. S. Sousa, H. Cho, B. Berger, J. Fellay, and J.-P. Hubaux. Truly privacy-preserving federated analytics for precision medicine with multiparty homomorphic encryption. *Nature Communications*, 12(1):5910, Oct 2021.
- [42] N. Gandhi, S. Mishra, S. K. Bharti, and K. Bhagat. Leveraging towards privacy-preserving using federated machine learning for healthcare systems. In 2021 IEEE International Conference on Electronics, Computing and Communication Technologies (CONECCT), pages 1–6, 2021.
- [43] A. Gascón, P. Schoppmann, B. Balle, M. Raykova, J. Doerner, S. Zahur, and D. Evans. Privacy-preserving distributed linear regression on high-dimensional data. PETS, 2017.
- [44] J. Geiping, H. Bauermeister, H. Dröge, and M. Moeller. Inverting gradients how easy is it to break privacy in federated learning? In NeurIPS, 2020.
- [45] I. Giacomelli, S. Jha, M. Joye, C. D. Page, and K. Yoon. Privacy-preserving ridge regression with only linearly-homomorphic encryption. In Springer ACNS, 2018.
- [46] R. Gilad-Bachrach, N. Dowlin, K. Laine, K. Lauter, M. Naehrig, and J. Wernsing. Cryptonets: Applying neural networks to encrypted data with high throughput and accuracy. In ICML, 2016.
- [47] V. Goyal, A. Polychroniadou, and Y. Song. Sharing transformation and dishonest majority mpc with packed secret sharing. Cryptology ePrint Archive, Paper 2022/831, 2022. https://eprint.iacr.org/2022/831.
- [48] S. Halevi and V. Shoup. Faster homomorphic linear transformations in helib. In H. Shacham and A. Boldyreva, editors, *Advances in Cryptology CRYPTO 2018*, pages 93–120, Cham, 2018. Springer International Publishing.
- [49] A. Hard, K. Rao, R. Mathews, F. Beaufays, S. Augenstein, H. Eichner, C. Kiddon, and D. Ramage. Federated learning for mobile keyboard prediction. CoRR, abs/1811.03604, 2018.
- [50] J. C. Heck and F. M. Salem. Simplified minimal gated unit variations for recurrent neural networks. In 2017 IEEE 60th International Midwest Symposium on Circuits and Systems (MWSCAS), pages 1593–1596, 2017.
- [51] M. Henaff, A. Szlam, and Y. LeCun. Recurrent orthogonal networks and long-memory tasks. In Proceedings of the 33rd International Conference on International Conference on Machine Learning - Volume 48, ICML'16, page 2034–2042. JMLR.org, 2016.
- [52] E. Hesamifard, H. Takabi, M. Ghasemi, and R. Wright. Privacy-preserving machine learning as a service. PETS, 2018.
- [53] B. Hitaj, G. Ateniese, and F. Perez-Cruz. Deep models under the GAN: Information leakage from collaborative deep learning. In ACM CCS, 2017.
- [54] S. Hochreiter and J. Schmidhuber. Long short-term memory. Neural computation, 9:1735–80, 12 1997.
- [55] S.-K. Hong, K. Gurjar, H.-S. Kim, and Y.-S. Moon. A survey on privacy preserving time series data mining. In 3rd International Conference on Intelligent Computational Systems, 2013.
- [56] Hourly Energy Consumption. https://www.kaggle.com/datasets/robikscube/hourly-energy-consumption. (Accessed: 2022-01-06).
- [57] Z. Huang, G. Zweig, M. Levit, B. Dumoulin, B. Oguz, and S. Chang. Accelerating recurrent neural network training via two stage classes and parallelization. In 2013 IEEE Workshop on Automatic Speech Recognition and Understanding, pages 326–331, 2013.
- [58] J. Jang, Y. Lee, A. Kim, B. Na, D. Yhee, B. Lee, J. H. Cheon, and S. Yoon. Privacy-preserving deep sequential model with matrix homomorphic encryption. In Proceedings of the 2022 ACM on Asia Conference on Computer and Communications Security, ASIA CCS '22, page 377–391, New York, NY, USA, 2022. Association for Computing Machinery.
- [59] B. Jayaraman, L. Wang, D. Evans, and Q. Gu. Distributed learning without distress: Privacy-preserving empirical risk minimization. In NeurIPS, 2018.
- [60] X. Jiang, M. Kim, K. Lauter, and Y. Song. Secure outsourced matrix computation and application to neural networks. In *Proceedings of the 2018 ACM SIGSAC Conference on Computer and Communications Security*, CCS '18, page 1209–1222, New York, NY, USA, 2018. Association for Computing Machinery.
- [61] X. Jin, P.-Y. Chen, C.-Y. Hsu, C.-M. Yu, and T. Chen. Cafe: Catastrophic data leakage in vertical federated learning. In NeurIPS, volume 34, pages 994–1006, 2021.
- [62] C. Juvekar, V. Vaikuntanathan, and A. Chandrakasan. Gazelle: A low latency framework for secure neural network inference. USENIX Security, 2018.
- [63] P. Kairouz, H. B. McMahan, B. Avent, A. Bellet, M. Bennis, A. N. Bhagoji, K. Bonawitz, Z. Charles, G. Cormode, R. Cummings, R. G. L. D'Oliveira, H. Eichner, S. E. Rouayheb, D. Evans, J. Gardner, Z. Garrett, A. Gascón, B. Ghazi, P. B. Gibbons, M. Gruteser, Z. Harchaoui, C. He, L. He, Z. Huo, B. Hutchinson, J. Hsu, M. Jaggi, T. Javidi, G. Joshi, M. Khodak, J. Konecný, A. Korolova, F. Koushanfar, S. Koyejo, T. Lepoint, Y. Liu, P. Mittal, M. Mohri, R. Nock, A. Özgür, R. Pagh, H. Qi, D. Ramage, R. Raskar, M. Raykova, D. Song, W. Song, S. U. Stich, Z. Sun, A. T. Suresh, F. Tramèr, P. Vepakomma, J. Wang, L. Xiong, Z. Xu, Q. Yang, F. X. Yu, H. Yu, and S. Zhao. Advances and open problems in federated learning. Foundations and Trends in Machine Learning, 14(1–2):1–210, 2021.
- [64] B. Kanuparthi, D. Arpit, G. Kerg, N. Ke, I. Mitliagkas, and Y. Bengio. h-detach: Modifying the lstm gradient towards better optimization. In 7th International Conference for Learning Representations (ICLR), 2019.
- [65] M. Keller and K. Sun. Secure quantized training for deep learning. In International Conference on Machine Learning, pages 10912–10938. PMLR, 2022.
- [66] V. Khomenko, O. Shyshkov, O. Radyvonenko, and K. Bokhan. Accelerating recurrent neural network training using sequence bucketing and multi-gpu data parallelization. In 2016 IEEE First International Conference on Data Stream Mining Processing (DSMP), pages 100–103, 2016.
- [67] B. Knott, S. Venkataraman, A. Hannun, S. Sengupta, M. Ibrahim, and L. van der Maaten. Crypten: Secure multi-party computation meets machine learning. In M. Ranzato, A. Beygelzimer, Y. Dauphin, P. Liang, and J. W. Vaughan, editors, *NeurIPS*, volume 34, pages 4961–4973. Curran Associates, Inc., 2021.
- [68] J. Konečny, H. B. McMahan, D. Ramage, and P. Richtárik. Federated optimization: Distributed machine learning for on-device intelligence. CoRR, abs:1610.02527, 2016.
- [69] J. Konecný, H. B. McMahan, F. X. Yu, P. Richtárik, A. T. Suresh, and D. Bacon. Federated learning: Strategies for improving communication efficiency. CoRR, abs/1610.05492, 2016.
- [70] K. Kursawe, G. Danezis, and M. Kohlweiss. Privacy-friendly aggregation for the smart-grid. In S. Fischer-Hübner and N. Hopper, editors, *Privacy Enhancing Technologies*, pages 175–191, Berlin, Heidelberg, 2011. Springer Berlin Heidelberg.
- [71] Q. V. Le, N. Jaitly, and G. E. Hinton. A simple way to initialize recurrent networks of rectified linear units. ArXiv, abs/1504.00941, 2015.
- [72] W. Li, F. Milletari, D. Xu, N. Rieke, J. Hancox, W. Zhu, M. Baust, Y. Cheng, S. Ourselin, M. J. Cardoso, and A. Feng. Privacy-preserving federated brain tumour segmentation. In *Springer MLMI*, 2019.
- [73] Y. Lindell. How to simulate it—a tutorial on the simulation proof technique. In Springer Tutorials on the Foundations of Cryptography. 2017.
- [74] R. Lindner and C. Peikert. Better key sizes (and attacks) for LWE-based encryption. In Springer Topics in Cryptology, 2011.
- [75] J. Liu, M. Juuti, Y. Lu, and N. Asokan. Oblivious neural network predictions via MiniONN transformations. In ACM CCS, 2017.
- [76] X. Liu and X. Yi. Privacy-preserving collaborative medical time series analysis based on dynamic time warping. In K. Sako, S. Schneider, and P. Y. A. Ryan, editors, *Computer Security – ESORICS 2019*, pages 439–460, Cham, 2019. Springer International Publishing.
- [77] X. Liu, Y. Zheng, X. Yi, and S. Nepal. Privacy-preserving collaborative analytics on medical time series data. *IEEE Transactions on Dependable and Secure Computing*, pages 1–1, 2020.
- [78] Y. Liu, J. J. Q. Yu, J. Kang, D. Niyato, and S. Zhang. Privacy-preserving traffic flow prediction: A federated learning approach. IEEE Internet of Things Journal, 7(8):7751–7763, 2020.
- [79] Y. Long, B. Wang, Z. Yang, B. Kailkhura, A. Zhang, C. A. Gunter, and B. Li. G-pate: Scalable differentially private data generator via private aggregation of teacher discriminators. CoRR, abs/1906.09338, 2021.
- [80] V. Lyubashevsky, C. Peikert, and O. Regev. On ideal lattices and learning with errors over rings. In EUROCRYPT, 2010.
- [81] B. McMahan, E. Moore, D. Ramage, S. Hampson, and B. A. y. Arcas. Communication-Efficient Learning of Deep Networks from Decentralized Data. In A. Singh and J. Zhu, editors, *Proceedings of the 20th International Conference on Artificial Intelligence and Statistics*, volume 54 of *Proceedings of Machine Learning Research*, pages 1273–1282. PMLR, 20–22 Apr 2017.
- [82] H. B. McMahan, D. Ramage, K. Talwar, and L. Zhang. Learning differentially private recurrent language models. In ICLR, 2018.
- [83] H. B. McMahan, D. Ramage, K. Talwar, and L. Zhang. Learning differentially private recurrent language models. CoRR, abs/1710.06963, 2018.

- [84] L. Melis, G. Danezis, and E. De Cristofaro. Efficient private statistics with succinct sketches. In Network and Distributed System Security Symposium (NDSS), 2016.
- [85] L. Melis, C. Song, E. De Cristofaro, and V. Shmatikov. Exploiting unintended feature leakage in collaborative learning. In *IEEE S&P*, 2019.
- [86] Lattigo: A library for lattice-based homomorphic encryption in go. https://github.com/ldsec/lattigo. (Accessed: 2022-01-06).
- [87] Mininet. http://mininet.org. (Accessed: 2022-01-06).
- [88] P. Mishra, R. Lehmkuhl, A. Srinivasan, W. Zheng, and R. A. Popa. Delphi: A cryptographic inference service for neural networks. In USENIX Security, 2020.
- [89] P. K. Mishra, D. Rathee, D. H. Duong, and M. Yasuda. Fast secure matrix multiplications over ring-based homomorphic encryption. *Information Security Journal:* A Global Perspective, 30(4):219–234, 2021.
- [90] P. Mohassel and P. Rindal. ABY3: a mixed protocol framework for machine learning. In ACM CCS, 2018.
- [91] P. Mohassel and Y. Zhang. SecureML: A system for scalable privacy-preserving machine learning. In IEEE S&P, 2017.
- [92] A. Molina-Markham, P. Shenoy, K. Fu, E. Cecchet, and D. Irwin. Private memoirs of a smart meter. In *Proceedings of the 2nd ACM Workshop on Embedded Sensing Systems for Energy-Efficiency in Building*, BuildSys '10, page 61–66, New York, NY, USA, 2010. Association for Computing Machinery.
- [93] C. Mouchet, E. Bertrand, and J.-P. Hubaux. An efficient threshold access-structure for rlwe-based multiparty homomorphic encryption. Cryptology ePrint Archive, Paper 2022/780, 2022. https://eprint.iacr.org/2022/780.
- [94] C. Mouchet, J. R. Troncoso-pastoriza, J.-P. Bossuat, and J. P. Hubaux. Multiparty homomorphic encryption from ring-learning-with-errors. PETS, 2021.
- [95] M. Nasr, R. Shokri, and A. Houmansadr. Comprehensive privacy analysis of deep learning: Passive and active white-box inference attacks against centralized and federated learning. In *IEEE S&P*, 2019.
- [96] V. Nikolaenko, U. Weinsberg, S. Ioannidis, M. Joye, D. Boneh, and N. Taft. Privacy-preserving ridge regression on hundreds of millions of records. In IEEE S&P, 2013.
- [97] A.-M. Olteanu, K. Huguenin, R. Shokri, M. Humbert, and J.-P. Hubaux. Quantifying interdependent privacy risks with location data. *IEEE Transactions on Mobile Computing*, 16(3):829–842, 2017.
- [98] N. Papernot, M. Abadi, Úlfar Erlingsson, I. Goodfellow, and K. Talwar. Semi-supervised knowledge transfer for deep learning from private training data. CoRR, abs/1610.05755, 2017.
- [99] N. Papernot, S. Song, I. Mironov, A. Raghunathan, K. Talwar, and U. Erlingsson. Scalable private learning with pate. In ICLR, 02 2018.
- [100] R. Pascanu, T. Mikolov, and Y. Bengio. On the difficulty of training recurrent neural networks. In *Proceedings of the 30th International Conference on International Conference on Machine Learning Volume 28*, ICML'13, page III–1310–III–1318. JMLR.org, 2013.
- [101] A. Patra and A. Suresh. Blaze: Blazing fast privacy-preserving machine learning. In NDSS, 2020.
- [102] L. T. Phong, Y. Aono, T. Hayashi, L. Wang, and S. Moriai. Privacy-preserving deep learning: Revisited and enhanced. In Springer ATIS, 2017.
- [103] L. T. Phong, Y. Aono, T. Hayashi, L. Wang, and S. Moriai. Privacy-preserving deep learning via additively homomorphic encryption. IEEE TIFS, 13(5):1333–1345, 2018.
- [104] A. Pyrgelis, E. De Cristofaro, and G. J. Ross. Privacy-friendly mobility analytics using aggregate location data. In *Proceedings of the 24th ACM SIGSPATIAL International Conference on Advances in Geographic Information Systems*, SIGSPACIAL '16, 2016.
- [105] D. Rathee, M. Rathee, G. R. K. Kiran, D. Gupta, R. Sharma, N. Chandran, and A. Rastogi. Sirnn: A math library for secure rnn inference. 2021 IEEE Symposium on Security and Privacy (SP), pages 1003–1020, 2021.
- [106] D. Rathee, M. Rathee, N. Kumar, N. Chandran, D. Gupta, A. Rastogi, and R. Sharma. CrypTFlow2: Practical 2-Party Secure Inference, page 325–342. 2020.
- [107] M. S. Riazi, M. Samragh, H. Chen, K. Laine, K. E. Lauter, and F. Koushanfar. Xonn: Xnor-based oblivious deep neural network inference. In USENIX Security, 2019.
- [108] D. E. Rumelhart, G. E. Hinton, and R. J. Williams. Learning representations by back-propagating errors. Nature, 323(6088):533-536, Oct 1986.
- [109] S. Sav, J.-P. Bossuat, J. R. Troncoso-Pastoriza, M. Claassen, and J.-P. Hubaux. Privacy-preserving federated neural network learning for disease-associated cell classification. *Patterns*, 3(5), 2022.
- [110] S. Sav, A. Pyrgelis, J. R. Troncoso-Pastoriza, D. Froelicher, J.-P. Bossuat, J. S. Sousa, and J.-P. Hubaux. Poseidon: Privacy-preserving federated neural network learning. In Network and Distributed System Security Symposium (NDSS), 2021.
- [111] A. M. Schäfer and H. G. Zimmermann. Recurrent neural networks are universal approximators. In S. D. Kollias, A. Stafylopatis, W. Duch, and E. Oja, editors, Artificial Neural Networks – ICANN 2006, pages 632–640, Berlin, Heidelberg, 2006. Springer Berlin Heidelberg.
- [112] P. Schoppmann, A. Gascon, M. Raykova, and B. Pinkas. Make some room for the zeros: Data sparsity in secure distributed machine learning. In ACM CCS, 2019.
- [113] E. Shi, T.-H. Chan, E. Rieffel, R. Chow, and D. Song. Privacy-preserving aggregation of time-series data. In *Network and Distributed System Security Symposium* (NDSS), volume 2, 01 2011.
- [114] Y. Shi, M.-Y. Hwang, K. Yao, and M. Larson. Speed up of recurrent neural network language models with sentence independent subsampling stochastic gradient descent. In *INTERSPEECH*, 2013.
- [115] R. Shokri and V. Shmatikov. Privacy-preserving deep learning. In *ACM CCS*, 2015.
- [116] R. Shokri, M. Stronati, C. Song, and V. Shmatikov. Membership inference attacks against machine learning models. In IEEE S&P, 2017.
- [117] R. Shokri, G. Theodorakopoulos, G. Danezis, J.-P. Hubaux, and J.-Y. Le Boudec. Quantifying location privacy: The case of sporadic location exposure. In S. Fischer-Hübner and N. Hopper, editors, *Privacy Enhancing Technologies*, pages 57–76, Berlin, Heidelberg, 2011. Springer Berlin Heidelberg.
- [118] R. Shokri, G. Theodorakopoulos, J.-Y. Le Boudec, and J.-P. Hubaux. Quantifying location privacy. In 2011 IEEE Symposium on Security and Privacy, pages 247–262, 2011.
- [119] Yahoo! Finance. https://finance.yahoo.com/lookup. (Accessed: 2022-01-06).
- [120] S. Tan, B. Knott, Y. Tian, and D. J. Wu. Cryptgpu: Fast privacy-preserving machine learning on the gpu. 2021 IEEE Symposium on Security and Privacy (SP), pages 1021–1038, 2021.
- [121] F. Tramèr, F. Zhang, A. Juels, M. K. Reiter, and T. Ristenpart. Stealing machine learning models via prediction {APIs}. In 25th USENIX security symposium (USENIX Security 16), pages 601–618, 2016.
- [122] S. Truex, N. Baracaldo, A. Anwar, T. Steinke, H. Ludwig, R. Zhang, and Y. Zhou. A hybrid approach to privacy-preserving federated learning. In ACM AISec, 2019.
- [123] S. Wagh, D. Gupta, and N. Chandran. Securenn: 3-party secure computation for neural network training. PETS, 2019.
- [124] S. Wagh, S. Tople, F. Benhamouda, E. Kushilevitz, P. Mittal, and T. Rabin. FALCON: Honest-majority maliciously secure framework for private deep learning. PETS, 2021.
- [125] A. Wainakh, F. Ventola, T. Müßig, J. Keim, C. Garcia Cordero, E. Zimmer, T. Grube, K. Kersting, and M. Mühlhäuser. User-level label leakage from gradients in federated learning. *PETS*, 2022:227–244, 04 2022.
- [126] Z. Wang, M. Song, Z. Zhang, Y. Song, Q. Wang, and H. Qi. Beyond inferring class representatives: User-level privacy leakage from federated learning. In *IEEE INFOCOM*, 2019.
- [127] K. Wei, J. Li, M. Ding, C. Ma, H. H. Yang, F. Farokhi, S. Jin, T. Q. S. Quek, and H. V. Poor. Federated learning with differential privacy: Algorithms and performance analysis. IEEE Transactions on Information Forensics and Security, 15:3454–3469, 2020.
- [128] M. Wen, R. Xie, K. Lu, L. Wang, and K. Zhang. Feddetect: A novel privacy-preserving federated learning framework for energy theft detection in smart grid. IEEE Internet of Things Journal, pages 1–1, 2021.
- [129] N. Wu, F. Farokhi, D. Smith, and M. A. Kaafar. The value of collaboration in convex machine learning with differential privacy. CoRR, abs/1906.09679, 2019.
- [130] Y. Yang, P. Gohari, and U. Topcu. On the privacy risks of deploying recurrent neural networks in machine learning. CoRR, abs/2110.03054, 2021.
- [131] J. Yoon, J. Jordon, and M. van der Schaar. PATE-GAN: Generating synthetic data with differential privacy guarantees. In *International Conference on Learning Representations*, 2019.
- [132] H. Zang and J. Bolot. Anonymization of location data does not work: A large-scale measurement study. In *Proceedings of the 17th Annual International Conference on Mobile Computing and Networking*, MobiCom '11, page 145–156. Association for Computing Machinery, 2011.

- [133] D. Zhang. Big data security and privacy protection. In Proceedings of the 8th International Conference on Management and Computer Science (ICMCS 2018), pages 275–278. Atlantis Press, 2018/10.
- [134] Q. Zhang, C. Wang, H. Wu, C. Xin, and T. V. Phuong. Gelu-net: A globally encrypted, locally unencrypted deep neural network for privacy-preserved learning. In Proceedings of the Twenty-Seventh International Joint Conference on Artificial Intelligence, IJCAI-18, pages 3933–3939. International Joint Conferences on Artificial Intelligence Organization. 7 2018.
- [135] Y. Zhang, G. Bai, X. Li, C. Curtis, C. Chen, and R. K. L. Ko. Privcoll: Practical privacy-preserving collaborative machine learning. In L. Chen, N. Li, K. Liang, and S. Schneider, editors, *Computer Security ESORICS 2020*, pages 399–418, Cham, 2020. Springer International Publishing.
- [136] B. Zhao, K. R. Mopuri, and H. Bilen. iDLG: Improved deep leakage from gradients. CoRR, abs/2001.02610, 2020.
- [137] W. Zheng, R. Deng, W. Chen, R. A. Popa, A. Panda, and I. Stoica. Cerebro: A platform for Multi-Party cryptographic collaborative learning. In 30th USENIX Security Symposium (USENIX Security 21), pages 2723–2740. USENIX Association, Aug. 2021.
- [138] W. Zheng, R. A. Popa, J. E. Gonzalez, and I. Stoica. Helen: Maliciously secure coopetitive learning for linear models. In IEEE S&P, 2019.
- [139] L. Zhu, Z. Liu, and S. Han. Deep leakage from gradients. In *NeurIPS*, volume 32. 2019.

APPENDIX A DETAILED DATASET DESCRIPTION

Hourly Energy Consumption (HEC): This dataset contains historical hourly energy consumption (in MegaWatts) from 12 major electricity distribution companies across the United States. The data was collected by PJM Interconnection LLC's website and is publicly available on Kaggle [56]. The dataset contains 12 files, each corresponding to a distribution company and to a specific time period. Table VI shows further details about the names of these 12 companies and the number of samples in each file. The total number of samples is 1,090,167. Note that for our experiments with N=10 data holders, we use the first 10 companies for the training, but we include samples from all companies in the test set. To capture the seasonality in energy consumption (i.e., trends with respect to daytime vs. nighttime, weekdays vs. weekends, winters vs. summers etc.), we incorporate on top of the energy consumption values 5 more features in the input space: hour, day-of-the-week, day-of-the-month, month and year (d=6). Additionally, for every file, we separately perform Min-Max scaling on the energy consumption values. This allows for a realistic distribution of the data among the multiple data holders (each data holder has one file, and does not necessarily know the range of the energy consumption values for other data holders).

Stock Prices (Stock): This dataset contains historical daily stock prices and statistics for 10 companies, and was collected by the Yahoo! Finance website [119]. Similar to the HEC dataset, we perform Min-Max scaling on each file separately. Table VII shows the company name for each file, the data collection period, and the number of samples per file. The total number of samples is 39,873.

To prepare the datasets for the forecasting tasks, we pre-process and slice them using a sliding window of size T for varying timesteps T = [5,10,20] for our model performance analysis.

Company Name	File Name [56]	#Samples
American Electric Power	[AEP_hourly.csv]	121,273
Commonwealth Edison	[COMED_hourly.csv]	66,497
The Dayton Power and Light C.	[DAYTON_hourly.csv]	121,275
Duke Energy Ohio/Kentucky	[DEOK_hourly.csv]	57,739
Dominion Virginia Power	[DOM_hourly.csv]	116,189
Duquesne Light Co.	[DUQ_hourly.csv]	119,068
East Kentucky Power Cooperative	[EKPC_hourly.csv]	45,334
FirstEnergy	[FE_hourly.csv]	62,874
Northern Illinois Hub	[NI_hourly.csv]	58,450
PJM East Region	[PJME_hourly.csv]	145,366
PJM West Region	[PJMW_hourly.csv]	143,206
PJM Load	[PJM_Load_hourly.csv]	32,896

TABLE VI: Detailed description of the HEC dataset.

APPENDIX B EXTENSIONS

Other RNN Architectures. In this work, we focus on simple RNN architectures with an input layer, hidden layers with RNN units, and an output layer of various structures, e.g., many-to-one, many-to-many, etc. We note that other RNN architectures, e.g., GRUs or LSTMs, comprise more complex pipelines that are harder to implement under (M)HE. Yet, RHODE's main building blocks, i.e., the approximated activation/clipping functions, the multi-dimensional packing, the matrix multiplication and transpose operations are sufficient to implement such complex RNN architectures. These RNN architectures, e.g., GRUs or LSTMs, require changes only on the Local Computation Phase of RHODE.

As an example, we summarize the protocol for the forward and backward pass of a GRU architecture in Algorithm 4. Such an RNN has the same workflow as a conventional RNN but with different operations inside the GRU unit. A typical GRU comprises an Update Gate

Company Name	File Name [119]	From	То	#Samples
Apple Inc.	[AAPL.csv]	1980-12-12	2017-08-11	9,247
Amazon.com, Inc.	[AMZN.csv]	1997-05-15	2022-05-19	6,296
Alibaba G.H.L.	[BABA.csv]	2014-09-19	2022-05-19	1,931
Facebook	[FB.csv]	2012-05-18	2022-05-19	2,518
Alphabet Inc.	[GOOG.csv]	2004-08-19	2022-05-19	4,470
Alphabet Inc.	[GOOGL.csv]	2004-08-19	2022-05-19	4,470
Netflix Inc.	[NFLX.csv]	2002-05-23	2022-05-19	5,034
Tesla, Inc.	[TSLA.csv]	2010-06-29	2022-05-19	2,995
Twitter, Inc.	[TWTR.csv]	2013-11-07	2022-05-19	2,148
Uber Tech., Inc.	[UBER.csv]	2019-05-10	2022-05-19	764

TABLE VII: Detailed description of the Stock dataset.

(R-Gate) that decides how much information from previous timesteps is needed for future timesteps, a Reset Gate (Z-Gate) that decides how much information to forget, and a Candidate activation (N-Gate) which is similar to the hidden state of an RNN unit. Other GRU variants modify these gates by computing only the bias or by excluding them [50], [33]. Both Reset and Update gates include an activation function that is typically a Sigmoid, $\varrho = \frac{1}{1+e^{-x}}$, and the hidden state includes an activation function that is typically Tanh, $\varphi = \frac{e^x - e^{-x}}{e^x + e^{-x}}$.

Given the above gate rules, the pipeline for the forward pass of a GRU is similar to a conventional RNN and the backward pass follows the BBPT algorithm with the chain rule for the calculation of the derivatives and the loss (see Algorithm 4). In more detail, the forward pass (Lines 4-11) comprises matrix multiplications, additions, and activation functions, thus, the packing scheme of RHODE, the matrix multiplication and the approximated building blocks can directly be applied. Similarly, the backward pass comprises the same operations as the forward pass but additionally requires multiple executions of the transpose operation, which is also supported by RHODE (Section V-A). Thus, different RNN architectures can be enabled using the main building blocks of RHODE. Yet, it is worth mentioning that the implementation of GRUs under MHE will increase RHODE's computation and communication overhead and its evaluation on more complex RNN architectures is a direction for future work.

Attacks Against PaaS. As discussed in Section IV, by retaining any information exchanged among the data holders and the final model encrypted, RHODE mitigates inference attacks that target the gradients/model updates exchanged during the FL training process [95], [85], [53], [139]. Nonetheless, inference attacks, e.g., model stealing [121] or membership inference [116], are also possible by exploiting the outputs of the PaaS. This is particularly the case for time-series applications (e.g., auto-regressive ones) where predictions (or queries) might be performed continuously over time. RHODE can minimize such leakage by feeding encrypted predictions back to the RNN for further oblivious processing and decrypt only an aggregated result (e.g., revealing only the time-series trend over a coarse period instead of a more fine-grained one). Additionally, such inference attacks against PaaS can be mitigated with mechanisms orthogonal to RHODE, e.g., by limiting the number of predictions a querier can request and/or by integrating a mechanism that perturbs the prediction outputs to obtain differential privacy guarantees.

Availability and Asynchronous Learning. In this work, we assume that all data holders are available (online) during the RHODE's training and prediction workflows. As we rely on a cross-silo federated learning setting, this assumption is realistic, yet, prohibitive in terms of failures as the collective cryptographic operations, e.g., $CBootstrap(\cdot)$ or $CKeySwitch(\cdot)$, require collaboration among all the data holders. Thus, to support asynchronous federated learning (driven by a time-threshold or by relying on a subset of online data holders), RHODE can be deployed with a threshold multi-party homomorphic encryption scheme which enables a subset of t-out-of-N data holders to perform the collective operations [93]. However, note that this cryptographic scheme would introduce a relaxation in RHODE's threat model (allowing collusions of up to t-1 data holders instead of N-1).

APPENDIX C MATRIX MULTIPLICATION PROTOCOL

Algorithm 5 presents the plaintext operations required for the matrix multiplication protocol with multi-dimensional packing (see Section V-A). This algorithm is described in the plaintext space for clarity; it is the same as Algorithm 3 with further details about the linear transformations employed. The first outer loop (Line 1) pre-computes the linear transformations on the entries (sub-matrices) of the right-matrix B while the second one (Line 9) calculates the entries of the left-matrix A. The inner loop starting at Line 15 computes the product between one entry of A and each corresponding row of B. Finally, it aggregates the intermediate results on the output C (Line 20).

APPROXIMATION OF THE PROPOSED CLIPPING FUNCTIONS

Figure 3 displays the approximation and error curves of $TanhClip(\cdot)$ and $SoftClip(\cdot)$ (compared to the baseline clipping function ($Clip(\cdot)$)) by employing the Minimax method with degrees $\mathfrak{p}=5$ and $\mathfrak{p}=15$ in the approximation interval [-30,30] and for a clipping threshold of

```
Algorithm 4 Local Computation Phase (GRU)
```

```
Input: U_z, U_r, U_n, W_z, W_r, W_n, V, b_u, b_z, b_r, b_n, h_{prev}, X = (x_1, x_2, \dots, x_t), Y = (y_1, y_2, \dots, y_t)
          Output: \nabla \mathbf{U}_z, \nabla \mathbf{U}_r, \nabla \mathbf{U}_n, \nabla \mathbf{W}_z, \nabla \mathbf{W}_r, \nabla \mathbf{W}_n, \nabla \mathbf{V}, \nabla \mathbf{b}_u,
\nabla \mathbf{b}_z, \nabla \mathbf{b}_r, \nabla \mathbf{b}_n
   1: loss \leftarrow 0
   2: \mathbf{h}_0 \leftarrow \mathbf{h}_{prev}
   3: for t \leftarrow 1:T do
                                                                                                                                                                                                                                                                                                                   ⊳ Forward Pass
                   \mathbf{z}_{raw} \leftarrow \mathbf{h}_{t-1} \times \mathbf{W}_z + x_t \times \mathbf{U}_z + \mathbf{b}_z
                                                                                                                                                                                                                                                                                                                                  ⊳ Z-Gate
   5:
                   \mathbf{z}_t \leftarrow \varrho(\mathbf{z}_{raw})
                   \mathbf{r}_{raw} \leftarrow \mathbf{h}_{t-1} \times \mathbf{W}_r + x_t \times \mathbf{U}_r + \mathbf{b}_r
                                                                                                                                                                                                                                                                                                                                 ⊳ R-Gate
   6:
                   \mathbf{r}_t \leftarrow \varrho(\mathbf{r}_{raw})
   7:
                   \mathbf{n}_{raw} \leftarrow (\mathbf{r}_t \odot \mathbf{h}_{t-1}) \times \mathbf{W}_n + x_t \times \mathbf{U}_n + \mathbf{b}_n
                                                                                                                                                                                                                                                                                                                                 ⊳ N-Gate
   8:
                   \mathbf{n}_t \leftarrow \varphi(\mathbf{n}_{raw})
   9:
10:
                   \mathbf{h}_t \leftarrow \mathbf{z}_t \odot \mathbf{h}_{t-1} + (1 - \mathbf{z}_t) \odot \mathbf{n}_t
                                                                                                                                                                                                                                                                                                                    ⊳ Hidden State
                   \mathbf{p}_t \leftarrow \mathbf{h}_t \times \mathbf{V} + \mathbf{b}_u
                                                                                                                                                                                                                                                                                                                     Dutput Gate
11:
12: end for
                                                                                                                                                                                                                                                                                                                    13: dh_{nxt} = 0
          \nabla \mathbf{U}_z, \nabla \mathbf{U}_r, \nabla \mathbf{U}_n, \nabla \mathbf{W}_z, \nabla \mathbf{W}_r, \nabla \mathbf{W}_n, \nabla \mathbf{V}
           \nabla \mathbf{b}_{u}, \nabla \mathbf{b}_{z}, \nabla \mathbf{b}_{r}, \nabla \mathbf{b}_{n} = \mathbf{0}
15: for t \leftarrow T : 1 do
                                                                                                                                                                                                                                                                                                              \mathbf{dy} \leftarrow \mathbf{p}_t - y_t
16:
                   \mathbf{dh} \leftarrow \mathbf{dy} \times \mathbf{V}^T + \mathbf{dh}_{nxt}
17:
                   \mathbf{dn} \leftarrow (1 - \mathbf{z}_t) \odot \mathbf{dh}
18:
                   \mathbf{dn}_{raw} \leftarrow \varphi'(\mathbf{n}_t) \odot \mathbf{dn} = (1 - n_t^2) \odot \mathbf{dn}
19:
                   \mathbf{dr} \leftarrow (\mathbf{dn}_{raw} \times \mathbf{W}_n^T) \odot \mathbf{h}_{t-1}
20:
                   \mathbf{dr}_{raw} \leftarrow \varrho'(\mathbf{r}_t) \odot \mathbf{dr} = \mathbf{r}_t \odot (1 - \mathbf{r}_t) \odot \mathbf{dr}
21:
22:
                   \mathbf{dz} \leftarrow (\mathbf{h}_{t-1} - \mathbf{n}_t) \odot \mathbf{dh}
                   \mathbf{dz}_{raw} \leftarrow \varrho'(\mathbf{z}_t) \odot \mathbf{dz} = \mathbf{z}_t \odot (1 - \mathbf{z}_t) \odot \mathbf{dz}
23:
                   \mathbf{dh}_h \leftarrow \mathbf{dh} \otimes \mathbf{z}_t
24:
                   \mathbf{dh}_z \leftarrow \mathbf{dz}_{raw} \times \mathbf{W}_z^T
25:
                   \mathbf{dh}_r \leftarrow \mathbf{dr}_{raw} \times \mathbf{W}_r^{\tilde{T}}
26:
                   \mathbf{dh}_n \leftarrow \mathbf{r}_t \otimes (\mathbf{dn}_{raw} \times \mathbf{W}_n^T)
27:
                   \mathbf{dh}_{nxt} \leftarrow \mathbf{dh}_z + \mathbf{dh}_h + \mathbf{dh}_n + \mathbf{dh}_r
28:
                    \nabla \mathbf{V} + = \mathbf{h}_t \otimes \mathbf{dy}
29:
                    \nabla \mathbf{U}_z + = x_t \otimes \mathbf{dz}_{raw}
30:
                    \nabla \mathbf{U}_r + = x_t \otimes \mathbf{dr}_{raw}
31:
                    \nabla \mathbf{U}_n + = x_t \otimes \mathbf{dn}_{raw}
32:
                    \nabla \mathbf{W}_z + = \mathbf{h}_{t-1} \otimes \mathbf{dz}_{raw}
33:
                    \nabla \mathbf{W}_r + = \mathbf{h}_{t-1} \otimes \mathbf{dr}_{raw}
34:
                    \nabla \mathbf{W}_n + = \mathbf{r}_t \odot (\mathbf{h}_{t-1} \otimes \mathbf{dn}_{raw})
35:
                    \nabla \mathbf{b}_{u} + = \mathbf{dy}
36:
                    \nabla \mathbf{b}_z + = \mathbf{d}\mathbf{z}_{raw}
37:
                    \nabla \mathbf{b}_r + = \mathbf{dr}_{raw}
38:
                    \nabla \mathbf{b}_n + = \mathbf{d}\mathbf{n}_{raw}
39.
40: end for
```

|m|=5. Error curves are plotted in the range of [-32,32] to observe the behavior of the approximations out of the approximation interval limits. E in the plot legends indicates the average absolute error of each function in the approximation interval [-30,30]. We observe that both approximations yield similar shapes and their error oscillation is alike. Yet, for smaller degrees, e.g., $\mathfrak{p}=5$, the average error E of $\mathsf{TanhClip}(\cdot)$ is slightly smaller than $\mathsf{SoftClip}(\cdot)$ (0.643 vs.0.706). For higher degrees ($\mathfrak{p}=15$), however, $\mathsf{SoftClip}(\cdot)$ achieves a better approximation (i.e., E=0.089 vs. E=0.183 for $\mathsf{TanhClip}(\cdot)$). Moreover, the divergence of $\mathsf{SoftClip}(\cdot)$ near the limits of the approximation interval is slower than $\mathsf{TanhClip}(\cdot)$ (see Figure 3c); this is a desired characteristic for any approximation. As a consequence, one should choose the approximation method based on the characteristics of the dataset, the desired degree (or precision) required for the polynomial approximation, and the aforementioned features of these approximations.

Algorithm 5 Matrix Multiplication

```
Inputs: A, B, two n \times n matrices, expressed as \ell \times \ell matrices, where each entry is a sub-matrix of dimension (n/\ell) \times (n/\ell).
Outputs: C \leftarrow A \otimes B
  1: for i=1 \rightarrow \ell do
             for j = 1 \rightarrow \ell do
  2:
                   \mathbf{b}_{i,j,1} \leftarrow \sigma(B_{i,j})
  3:
                    for v=2\rightarrow n/\ell do
  4:
  5:
                          \mathbf{b}_{i,j,v} \leftarrow \psi_v(\mathbf{b}_{i,1})
                    end for
  6:
             end for
  7:
  8: end for
  9: for i = 1 \rightarrow \ell do
             for j = 1 \rightarrow \ell do
10:
                   \mathbf{a}_1 \leftarrow \tau(A_{i,j})
11:
                    for v=2\rightarrow n/\ell do
12:
                          \mathbf{a}_v \leftarrow \phi_v(\mathbf{a}_1)
13:
                    end for
14:
                    for v = 1 \rightarrow \ell do
15:
                          d \leftarrow \mathbf{a}_1 \odot \mathbf{b}_{j,1}
16:
                          for k=2\rightarrow n/\ell do
17:
                                d \leftarrow d + \mathbf{a}_k \odot \mathbf{b}_{j,k}
18:
                          end for
19:
                          C_{i,v} \leftarrow C_{i,v} + d
20:
                    end for
21:
             end for
22:
23: end for
```

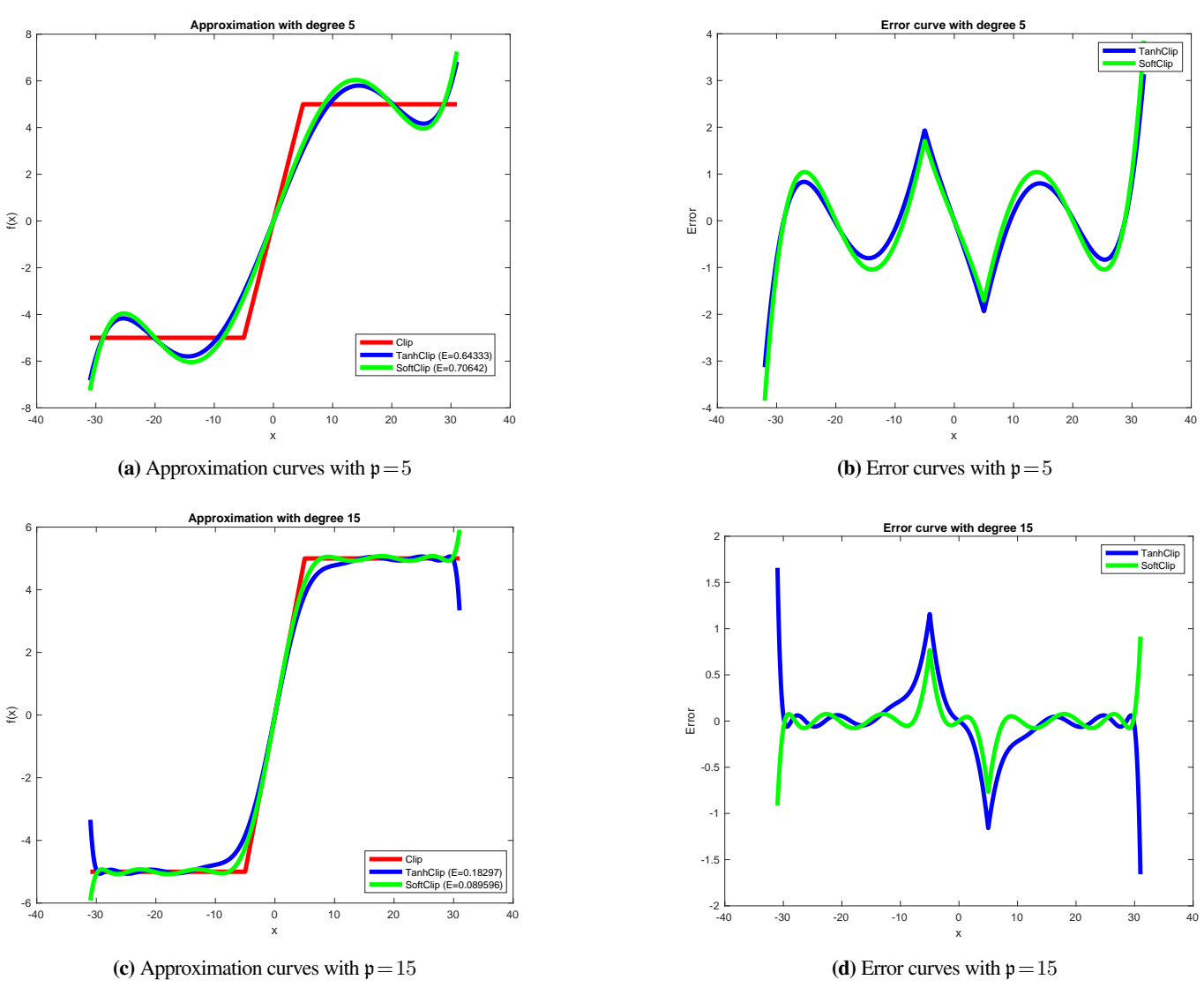


Figure 3: Approximation and error curves of $TanhClip(\cdot)$ and $SoftClip(\cdot)$ compared to baseline clipping function $Clip(\cdot)$ with degrees $\mathfrak{p}=5$ and $\mathfrak{p}=15$ in the interval [-30,30] for a clipping threshold of |m|=5. Error curves are plotted in the range of [-32,32]. E in the legends of the approximation plots indicates the average absolute error per approximation in the interval [-30,30].